



## Article

# Tropically Adapted Passive Building: A Descriptive-Analytical Approach Using Multiple Linear Regression and Probability Models to Predict Indoor Temperature

Siti Fatimah Salleh <sup>1,\*</sup>, Ahmad Abubakar Suleiman <sup>2,3</sup> , Hanita Daud <sup>2</sup>, Mahmud Othman <sup>4</sup> ,  
Rajalingam Sokkalingam <sup>2</sup> and Karl Wagner <sup>5</sup>

<sup>1</sup> PETRONAS Research Sdn. Bhd., Off Jalan Ayer Itam, Kawasan Institusi Bangi, Kajang 43000, Malaysia

<sup>2</sup> Fundamental and Applied Sciences Department, Universiti Teknologi PETRONAS, Seri Iskandar 32610, Malaysia; ahmad\_22000579@utp.edu.my (A.A.S.); hanita\_daud@utp.edu.my (H.D.); raja.sokkalingam@utp.edu.my (R.S.)

<sup>3</sup> Department of Statistics, Aliko Dangote University of Science and Technology, Wudil 713281, Nigeria

<sup>4</sup> Department of Information System, Universitas Islam Indragiri, Tembilahan 29212, Indonesia; mahmod.othman@unisi.ac.id

<sup>5</sup> Faculty of Business Administration, Rosenheim Technical University of Applied Sciences, Hochschulstraße, 83024 Rosenheim, Germany; karl.wagner@fh-rosenheim.de

\* Correspondence: sitifatimah.salleh@petronas.com

**Abstract:** The quest for energy efficiency in buildings has placed a demand for designing and modeling energy-efficient buildings. In this study, the thermal energy performance of a tropically adapted passive building was investigated in the warm tropical climate of Malaysia. Two mock-up buildings were built to represent a “green”, made of clay brick double-glazed passive building and a conventional, made of concrete “red” building. The mean indoor temperature of the passive building was found to be always lower than that of the red building throughout the experiment during different weather constellations. Our research builds upon existing work in the field by combining multiple linear regression models and distribution models to provide a comprehensive analysis of the factors affecting the indoor temperature of a building. The results from the fitted multiple linear regression models indicate that walls and windows are critical components that considerably influence the indoor temperature of both passive buildings and red buildings, with the exception of passive buildings during the hot season, where the roof has a greater influence than the window. Furthermore, the goodness-of-fit test results of the mean indoor temperature revealed that the Fréchet and Logistic probability models fitted the experimental data in both cold and hot seasons. It is intended that the findings of this study would help tropical countries to devise comfortable, cost-effective passive buildings that are green and energy efficient to mitigate global warming.

**Keywords:** passive building; green building; energy saving; thermal comfort; windows; regression analysis; probability distribution; logistic distribution; Fréchet distribution



**Citation:** Salleh, S.F.; Suleiman, A.A.; Daud, H.; Othman, M.; Sokkalingam, R.; Wagner, K. Tropically Adapted Passive Building: A Descriptive-Analytical Approach Using Multiple Linear Regression and Probability Models to Predict Indoor Temperature. *Sustainability* **2023**, *15*, 13647. <https://doi.org/10.3390/su151813647>

Academic Editors: Valentín Molina-Moreno, Pedro Núñez-Cacho, Jarosław Górecki, Mohamad Achour and Arnaud Diemer

Received: 27 June 2023

Revised: 26 August 2023

Accepted: 28 August 2023

Published: 12 September 2023



**Copyright:** © 2023 by the authors. Licensee MDPI, Basel, Switzerland. This article is an open access article distributed under the terms and conditions of the Creative Commons Attribution (CC BY) license (<https://creativecommons.org/licenses/by/4.0/>).

## 1. Introduction

For more than a century, the use of fossil fuels, along with uneven and unsustainable energy and land use, has resulted in 1.1 °C of global warming over pre-industrial levels [1]. Natural catastrophes are on the rise because of climate change and increasingly severe weather patterns, endangering both the environment and people globally. In 2019, energy, industry, transportation, and buildings accounted for around 79% of global GHG emissions, while agriculture, forestry, and other land use (AFOLU) accounted for 22% [1]. Furthermore, building operations in 2021 accounted for 27% of all energy sector emissions and 30% of the world’s final energy consumption, with 8% of those emissions coming directly from buildings and 19% coming indirectly via the generation of power and heat those structures utilized [2]. Therefore, urban energy planning and management should

focus on developing a solid framework of principles for reducing building energy use patterns. While minimum performance standards and building energy codes are becoming more comprehensive and stringent, and more efficient and renewable energy technologies are being adopted in buildings, the International Energy Agency (IEA) claims that the construction industry needs to transform more quickly to meet the Net Zero Emissions by 2050 Scenario [2]. To attain this goal, research on practical solutions for energy-efficient building design that caters to its surroundings and natural climate is required to mitigate their environmental impacts.

The primary objective of every building is to provide essential comfort in the indoor environment. Increased humidity and heat absorption from external temperature, particularly in hot and arid climate regions, will result in discomfort and an increase in active cooling demand, as well as HVAC-related energy usage. By 2050, about two-thirds of homes worldwide will have air conditioners [3]. Most of the contributions come from the world's hotter regions, namely China, India, and Indonesia, which together account for more than half of the total. The highest upper space limit (USL) of worldwide tropical standards for thermal comfort, according to the American Society of Heating, Refrigerating, and Air-Conditioning Engineers (ASHRAE), is 26.1 °C (without velocity) or 28.6 °C (with velocity of bearable 0.7 m/s effects in −2.5 °C). The heat transmitted into or lost from a building fluctuates according to the temperature shift from day to night, as well as variations in the weather, such as heating using sunlight and cooling using wind or rain. Understanding the thermal response of the building envelope to the external environment is crucial to preserve indoor thermal comfort or, at the very least, to minimize cooling demand in tropical climates.

The concept of passive building has been around for several decades in creating energy-efficient buildings that require minimal heating and cooling systems. Its common tactics for creating a comfortable indoor atmosphere include non-mechanical methods of passive solar design, insulation, and induced ventilation techniques [4]. Passive solar design entails optimizing the orientation and shading using roof cover, overhangs, awnings, trees, vegetation, etc. It was discovered that solar passive design based on the thermophysical characteristics and design of building envelopes may successfully eliminate two-thirds of the discomfort [5]. Insulating materials could also be applied to the outside face of a wall or roof such that the thermal mass of the wall is poorly linked with the outside source and firmly coupled with the inside. Sustainable biopolymer composites have been researched with the use of organic fibers like coir [6,7]. A coir–cement composite used as an insulator was found to reduce thermal conductivity by 0.16–0.19 W/mK [8]. Further, induced ventilation techniques including solar chimney and air vents are beneficial to exhaust hot air from the building at a quick rate.

The mean indoor temperature under free-running natural ventilation normally ranges from 27 °C to 37 °C [9]. Monitoring indoor temperature is essential for assessing building thermal efficiency (i.e., thermal transmittance (U-value) of the building envelope) and potentially upgrading the energy-efficient options towards energy conservation. There are several effective methods and technologies available for these purposes. One common approach involves using temperature sensors such as thermocouples, resistance temperature detectors (RTDs), and thermistors, which provide accurate readings based on electrical changes. Additionally, infrared (IR) thermometers offer non-contact temperature measurement using thermal radiation detection. Meanwhile, deploying wireless sensor networks such as IoT sensors throughout the building allows real-time temperature monitoring and data transmission to a central hub for analysis. However, this typically comes with a significantly elevated cost.

The simulation technique is a useful tool for the designers to achieve an optimum thermal performance of the localized buildings under a given thermal climate. Energy modeling and optimization were utilized to find the best solution based on the pre-defined design requirements [10]. In another study, a re-designed school building, which used passive design strategies rather than active design strategies, had a lower final energy than the

original school design, which used active design strategies [11]. The findings support the hypothesis that excessive use of active methods in construction may be counterproductive, and passive building design techniques should be prioritized since they are more energy efficient than active solutions. Micro-site analyses in relation to thermal impacts on the building performance can be easily achieved by using physical modeling techniques [12]. In order to investigate the thermal simulation of a full-sized passive solar building using scale models, researchers constructed a simplified single test room, and several test units of half and quarter-scale were used. Using the thermal scaling technique, all the analyses of the test results suggested that it is quite feasible to simulate the thermal performance of full-scale passive buildings. Thus, one of the simple ways to simulate the thermal performance of the building is to take a single-room, small-scale physical model under computer-simulated weather and solar radiation conditions [13]. It aids in determining the overheating time and appropriate mitigating methods, such as a moveable sunshade [14].

However, all the abovementioned simulation methods involve tedious calculations, which in turn increase computation time. Furthermore, practical experimentation in a real-world situation is required to validate the concept. The purpose of this study is to determine the effect of passive architectural design on the indoor or indoor temperature in a real mock-up residential structure modeled after a passive building (PB). PB was built by using a passive building enclosure design, which includes the use of sustainable materials in the construction of roofs, floors, walls, and windows. The focus is to observe how they interact with one another within the system rather than analyzing the impact of separate components. The tropical thermal comfort USL of 28.6 °C was used as the tropical residential thermal comfort (TRTC) benchmark.

In recent years, there have been notable advancements in the field of statistical analysis within environmental studies, particularly in the utilization of probability distribution models [15]. These statistical models have proven to be valuable decision-support tools for assessing temperature patterns. The use of probability distribution models in the statistical modeling of extreme hydrological and climatic phenomena has a long history and is one of the latest advances in the statistical analysis of environmental studies. For instance, several researchers compared many probability distributions to find the one that best fits the empirical datasets. A study in Australia showed that the normal and generalized extreme value distributions fit the yearly maximum temperature data the best [16]. Furthermore, probability distribution models were also applied to model the monthly maximum temperatures in Bangladesh [17,18] and the average daily maximum temperature of South Africa [19] and Thailand [20]. Another study applied five probability models, such as the Weibull, Gumbel, Cauchy, Logistic, and normal distribution, to determine the best fit for the temperature data [21]. The daily maximum and minimum temperatures of three cities were modeled using a mixture Gaussian distribution [22]. In another study, five probability distributions, such as log-normal, Gumbel, logistic, Weibull, and log-logistic distributions, were applied over a range of temperatures [23]. Moreover, five probability distributions, including gamma, Gumbel, log-normal, normal, and Weibull distributions were applied to model the annual maximum temperature in the Northwest Himalayan region of India [24].

Further, distribution modeling is important and influential in the fields of rainfall and food frequency analysis. Many researchers have estimated extreme rainfall events and flood occurrences. For instance, a study focused on modeling excessive daily rainfall in several locations in Italy [25]. When compared to light-tailed distributions, their results showed that heavy-tailed distributions offer a more precise estimate of the maximum daily rainfall values. In another study, two types of distributions, namely Gumbel extreme value type-I and Log Pearson type-III, were applied to model the magnitude and frequency of food events in Narmada River, India [26]. In another research, three different probability distributions were employed for modeling the peak discharge of the Jhelum River [27]. In a study to model the monthly rainfall data in Brazil [28], eight probability models and six goodness-of-fit tests included the Akaike information criterion. Additionally, they employed the maximum likelihood method to estimate the parameters of the distributions. A

study was carried out on food frequency analysis at the Ume River in Sweden to determine the maximum water flow for various future timeframes or return periods [29].

Moreover, many researchers in the field of wind energy have used probability distributions to analyze and model many aspects of its generation and utilization. For instance, distribution models were employed to evaluate the hourly wind speed data from various locations in Pakistan [30]. Similarly, wind speed data recorded in Slovakia were used to determine the best-fitting distribution [31]. Groundwater quality is essential for the health of humans, animals, and plants. In the field of groundwater monitoring, researchers extensively use probability distributions to analyze and model groundwater data for effective monitoring. For instance, five probability distributions were employed to assess the calcium concentrations of groundwater data in Kano State, Nigeria [32]. A similar study was conducted to evaluate the chemical parameters of groundwater using six probability distributions, such as normal, log-normal, gamma, Weibull, logistic, and log-logistic distributions [33]. The following studies can be referred to for more probability distribution modeling works [34–52].

In the present study, three distribution models, namely Fréchet, Gamma, and Logistic distributions, were utilized to model the mean indoor temperature PB and RB temperatures during cold and hot seasons in Malaysia. To the best of the authors' knowledge, this is the first ever reported comparative statistical study of the influence of passive green design in its entirety on indoor temperature using three probability distributions and a significant number of goodness-of-fit tests. The primary objectives and justification of this study are as follows:

- (i) to investigate the impact of passive architectural design on indoor temperature regulation within a physical mock-up of a residential structure that closely emulates the principles of a passive building (PB).
- (ii) to evaluate and compare the thermal performance of the PB and RB mock-ups using a descriptive-analytical approach, focusing on the utilization of multiple linear regression (MLR) models and distribution models. By leveraging MLR models, the study aims to identify key variables that significantly influence indoor temperature variations, shedding light on the effectiveness of passive design elements. Furthermore, distribution models will enable the exploration of temperature distribution patterns within the mock-up, unveiling insights into the spatial dynamics of temperature control of residential buildings in warm tropical climates.
- (iii) to provide an in-depth understanding of the intricate relationships between various architectural factors and indoor temperature fluctuations. Using this multifaceted approach, the study endeavors to advance our comprehension of how passive architectural design strategies impact indoor thermal comfort, fostering informed decision-making for sustainable building design practices.

The rest of the paper is structured as follows. Section 2 describes the experiment methodologies and statistical analysis conducted. Section 3 presents the results and discussion. Finally, Section 4 provides the conclusion of the study.

## 2. Materials and Methods

Figure 1 describes the methodologies employed in this work. The experimental data sets were collected in Malaysia, which consisted of PB and RB temperature variations in cold and hot seasons. To acquire a “bird’s eye view” of the experimental outcomes, statistical descriptive analysis using a boxplot was used. Next, correlation analysis was employed to determine the relationship between building enclosures’ temperatures. A multiple linear regression model was built in order to estimate the indoor temperature across the wall, roof, floor, and window temperatures. R-squared and adjusted R-squared values were used to evaluate the performance of the implemented models, and then graphical representations of the important model parameters were presented. Finally, three important probability distributions, Fréchet, Gamma, and Logistic distributions, are employed to assess the mean indoor temperatures of PB and RB in cold and hot seasons.

The log-likelihood, Akaike information criterion (AIC), Bayesian information criterion (BIC), and Kolmogorov–Smirnov (K-S) tests are employed to determine the best fit of the probability distribution model for the mean indoor temperature.

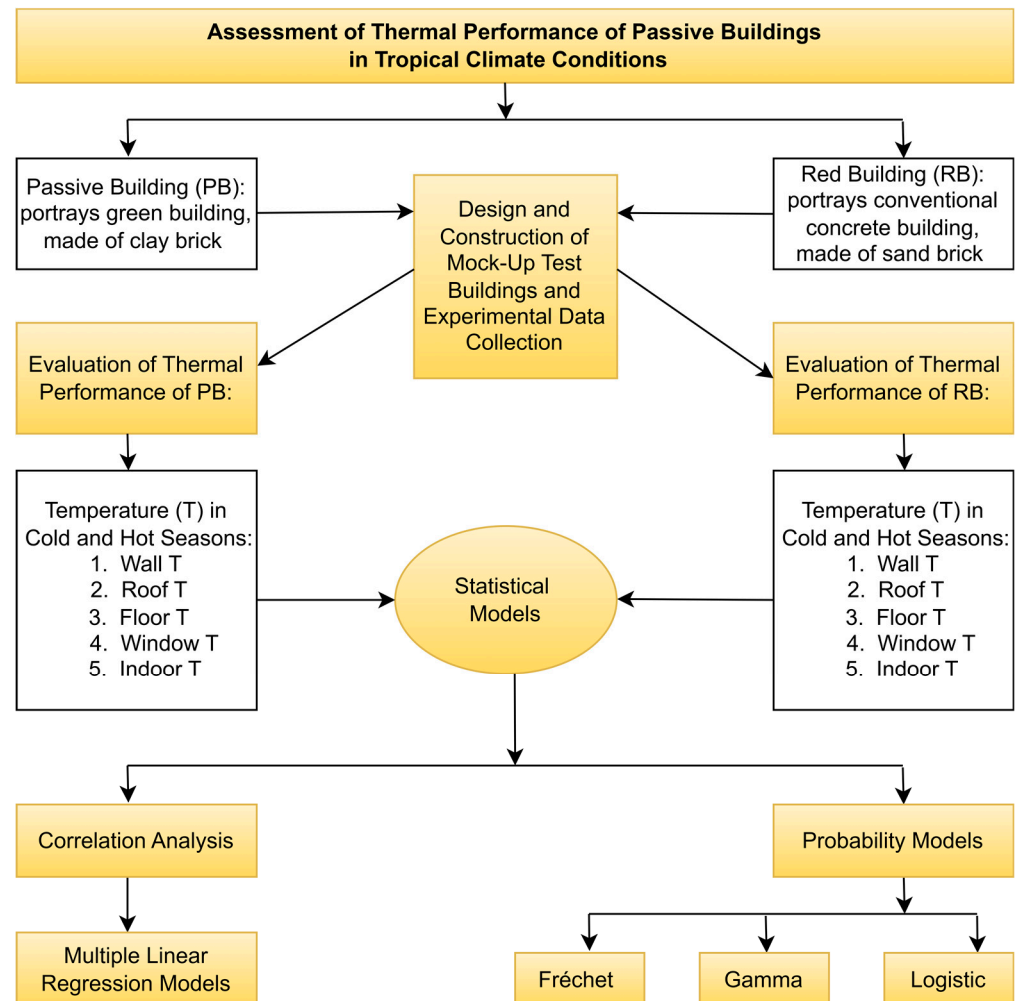


**Figure 1.** Flow chart of the methodology of the work.

### 2.1. Mock-Up Buildings Setup



The project entails the creation of two mock-up buildings: (i) a passive building (PB) to symbolize a “green” design building made of clay bricks and (ii) a red building (RB) with a conventional building made of concrete with conventional design. Each mock-up with proportions of 3 m high, 3 m wide, and 3 m deep was built as a life lab or room where a person may stand, sit, and even sleep. The average window-to-wall ratio is 31% east, south, and west and 0% north. The PB walls are constructed of double-layer clay bricks. Meanwhile, the RB portrays the common, typical control unit of a standard low-cost house made of basically sand–cemented bricks or concrete. Further details of the design of both buildings are provided in Table 1 below.

For the purposes of the experiment, we closed the single-glazed windows in the RB in order to assess the influence of the double-glazed windows of PB. In each building, we obtained five distinct temperatures, including wall, roof, floor, window, and indoor temperature, to test the interplay of all building enclosures toward the indoor temperature in a system of a tropically adapted from the passive house.

The surface temperatures were measured using a robust and practical infrared thermometer (VOLTCRAFT IR 500-12D, Conrad Electronic International GmbH & CoKg Durisolstraße, Wels, Austria) with a pistol grip for contactless measurement of temperatures. The surface temperatures of each building envelope include interior walls, windows,

roofs, and floor surfaces. This equipment was sourced from Conrad Electronic International GmbH & CoKg Durisolstraße, 24600 Wels, Austria. Three readings were taken manually from 5 measurement points of each surface and were noted down to calculate the average to reduce the impact of small fluctuations or measurement errors. Meanwhile, the indoor temperature was measured using a digital VOLTcraft K202 thermometer sensor equipped with a datalogger and positioned in the middle of the room, with all windows and doors firmly closed. The Voltcraft thermometers were properly calibrated according to the manufacturer's instructions and kept clean and free from any debris or contaminants. For both surface temperature and indoor temperature, the time interval is 30 min, taken every day for 12 h from 8 am to 8 pm for 2 months of the hot season and cool season.

**Table 1.** Architectural design of mock-up passive building (PB) and red building (RB).

| Building Type /Enclosures | Passive Building (PB)   | Red Building (RB)   |
|---------------------------|---|---|
|                           |    |    |
| Wall                      | Clay brick, double wall with 2 cm gap.  | Sand-cemented brick, single wall.   |
| Roof                      | Red clay brick tiles (15 mm).   | Metal cladding roof (coated).   |
| Floor                     | Wood wool cement board.   | Wood wool cement board.   |
| Window                    | Double glazing with UPVC window frame and external shutters.  | Single glazing with aluminum window frame.  |
| Other features            | <ul style="list-style-type: none"> <li>• Almost airtight</li> <li>• High insulation capability walls</li> <li>• Ventilated and insulated roof (5 cm Duralite ceiling)</li> <li>• Solar panels for LED lighting</li> </ul> | <ul style="list-style-type: none"> <li>• Open air (closed for experiment)</li> <li>• Uninsulated wall</li> <li>• Uninsulated roof (0.42 mm metal deck)</li> <li>• Fluorescent lights</li> </ul> |

The mock-up buildings are located in Selangor, Malaysia, at the British–Malaysian Institute of Universiti Kuala Lumpur (BMI-UniKL) with a tropical climate. The experiment was carried out across a number of months, which can be categorically divided into two categories: (i) hot/dry season (March to April 2016), with most cloudy-sunny days and little to no significant rain interception, and (ii) cold season (October to November 2016) with the monsoon season's most rainy days.

## 2.2. Statistical Analysis

### 2.2.1. Descriptive Analysis

The properties of a dataset were enumerated and described using descriptive statistics to provide an overview of the experiment results. Box plots are particularly useful for highlighting the dataset's median, quartiles, and outliers. They were used to examine the distributions of the RB and PB datasets across the hot and cold seasons, as well as to assess a dataset's central tendency, dispersion, and skewness.

### 2.2.2. Correlation Analysis

Correlation is a technique that measures the nature, degree, and extent of association existing between two continuous variables. Karl Pearson's correlation coefficient ( $r$ ) is

a measure of the degree of relationship between two variables  $\theta$  and  $\eta$  [53], which is expressed as given in Equation (1).

$$r = \frac{n \left( \sum_{i=1}^n \theta_i \eta_i \right) - \left( \sum_{i=1}^n \theta_i \right) \left( \sum_{i=1}^n \eta_i \right)}{\sqrt{\left[ n \sum_{i=1}^n \theta_i^2 - \left( \sum_{i=1}^n \theta_i \right)^2 \right] \cdot \left[ n \sum_{i=1}^n \eta_i^2 - \left( \sum_{i=1}^n \eta_i \right)^2 \right]}}, \quad (1)$$

where  $n$  is the number of observations, and the  $r$  values are between  $-1$  and  $1$ ; a positive value indicates a positive relationship, while a negative value is a negative association of variables. A value  $r = 0$  is an indicator of a negligible relationship between variables [54]. The study by [55] designated the correlation values as ‘moderate’ and ‘strong’ concerning the  $r$  values of  $0.5$ – $0.7$  and  $>0.7$ , respectively. The correlation value ( $r < 0.5$ ) values implies a weak correlation.

This technique was applied to correlate groundwater pollutants in the investigated areas. The correlation of groundwater parameters is computed to identify the contribution amount of association of each parameter contributed to the groundwater contamination [56].

### 2.2.3. Regression Analysis Using Multiple Linear Regression Model

Regression analysis is used to develop a mathematical relationship between dependent and independent variable(s). Here, regression analysis was applied to establish a predictive relation between the indoor temperature of four other building enclosure temperatures, such as wall, roof, floor, and window, for cool and hot seasons. An important parameter in estimating a good fit for the model is the coefficient of determination or simply adjusted R-squared. The adjusted R-squared number of properties makes it a more suitable measure of goodness-of-fit than R-squared [57]. The choice of dependent and independent variables in a regression model is crucial. A multiple linear regression approach is used to develop a relationship between the indoor temperature as the dependent variable and building enclosure temperatures, namely wall, roof, floor, and window as the independent variables.

Basically, while developing the model, we iteratively analyze the variables for

- i. Normality of distribution
- ii. Extreme values
- iii. Multiple collinearity
- iv. Homoscedasticity (even distribution of residuals)
- v.  $p$ -value of coefficients and R-squared/F-statistic of the model.

In addition, we split the data into training and validation samples. We used 80% for training and 20% for validation.

The multiple regression model can be implemented as follows:

$$\eta = \omega_0 + \omega_1 \theta_1 + \omega_2 \theta_2 + \dots + \omega_k \theta_k + \varepsilon, \quad (2)$$

where  $\eta$  = dependent variable,

$\omega_i$  = regression parameters,  $i = 1, 2, \dots, n$ ,

$\theta_i$  = independent variables,  $i = 1, 2, \dots, n$ ,

$\varepsilon$  = error term assumed to be *i.i.d*  $N(0, \sigma^2)$ .

More details on the regression model are provided in [58,59].

Let  $\eta_1, \eta_2, \dots, \eta_n$  be  $n$  dependent observations on  $\eta$ . Then, each of observations  $\eta_i$  can be written as

$$\eta_i = \omega_0 + \omega_1 \theta_{i1} + \omega_2 \theta_{i2} + \dots + \omega_k \theta_{ik} + \varepsilon, \quad (3)$$

where  $\theta_{ij}$  is the  $j^{\text{th}}$  independent variable for the  $i^{\text{th}}$  observation,  $i = 1, 2, \dots, n$ . It is sometimes advantageous to introduce matrices to study the linear equation. Let  $\theta_0 = 1$ . Define the following matrices:

$$\theta = \begin{bmatrix} \theta_0 & \theta_{11} & \theta_{12} & \dots & \theta_{1k} \\ \theta_0 & \theta_{21} & \theta_{22} & \dots & \theta_{2k} \\ \vdots & \vdots & \vdots & \ddots & \vdots \\ \theta_0 & \theta_{n1} & \theta_{n2} & \dots & \theta_{nk} \end{bmatrix}, \quad \eta = \begin{bmatrix} \eta_1 \\ \eta_2 \\ \vdots \\ \eta_n \end{bmatrix}, \quad (4)$$

$$\omega = \begin{bmatrix} \omega_0 \\ \omega_1 \\ \vdots \\ \omega_n \end{bmatrix}, \quad \text{and} \quad \varepsilon = \begin{bmatrix} \varepsilon_1 \\ \varepsilon_2 \\ \vdots \\ \varepsilon_n \end{bmatrix}.$$

Thus, the  $n$  equations representing the linear equations can be rewritten in the matrix form as  $\eta = \theta\omega + \varepsilon$ .

#### 2.2.4. Probability Distributions of Mean Indoor Temperature

Uncertain phenomena refer to outcomes that cannot be precisely predicted with certainty. Seasonal variations contribute to the uncertainty associated with events like extreme temperatures. Developing suitable probability distribution models that address uncertainties is essential for accurately characterizing such events. These models serve as valuable future reference guides for monitoring temperature changes in any study area of interest. In this study, we focus on the mean indoor temperature readings, denoted as the random variable  $X$ , and define it using specific probability distribution functions. The probability distributions used in this research study include the Fréchet, gamma, and logistic distributions. Brief reviews of these distributions are discussed in the following paragraphs.

##### (i) Fréchet Distribution

A random variable  $X$  is a Fréchet distribution with the shape parameter  $\alpha$  and the rate parameter  $\beta$  if its pdf is given by:

$$f(x; \alpha, \beta) = \alpha\beta^\alpha x^{-\alpha-1} \exp\left(-\left(\frac{\beta}{x}\right)^\alpha\right), \quad x > 0; \quad \alpha > 0, \beta > 0. \quad (5)$$

The mean and variance of the Fréchet distribution are, respectively given as:

$$E(X) = \beta\Gamma\left(1 - \frac{1}{\alpha}\right) \text{ for } \alpha > 1 \text{ and } \text{Var}(X) = \beta\left(\Gamma\left(1 - \frac{2}{\alpha}\right) - \left(\Gamma\left(1 - \frac{1}{\alpha}\right)\right)^2\right) \text{ for } \alpha > 2.$$

##### (ii) Gamma Distribution

A random variable  $X$  is a Gamma distribution with the shape parameter  $\alpha$  and the rate parameter  $\beta$ , if its pdf is given by:

$$f(x; \alpha, \beta) = \frac{\beta^\alpha}{\Gamma(\alpha)} x^{\alpha-1} \exp(-\beta x), \quad x > 0, \alpha > 0, \beta > 0. \quad (6)$$

The mean and variance of the Gamma distribution are, respectively given as:

$$E(X) = \frac{\alpha}{\beta} \text{ and } \text{Var}(X) = \frac{\alpha}{\beta^2}$$



### (iii) Logistic Distribution

A random variable  $X$  is said to follow a Logistic distribution with the location parameter  $\mu$  and the scale parameter  $s$ , if its pdf is given by:

$$f(x; \mu, s) = \frac{\exp - \left( \frac{x - \mu}{s} \right)}{s \left( 1 + \exp - \left( \frac{x - \mu}{s} \right) \right)^2}, \quad x \in \mathbb{R}, \mu \in \mathbb{R}, s > 0. \quad (7)$$

The mean and variance of the logistic distribution are, respectively given as:

$$E(X) = E \left( \mu + s \left( \frac{x - \mu}{s} \right) \right) \text{ and } Var(X) = \frac{s^2 \pi^2}{3}. \quad (8)$$

### 2.2.5. Probability Distribution Tests

In statistical hypothesis testing, one assesses whether sample data are derived from a population that follows a predicted probability distribution. This involves selecting a model to fit a probability distribution to a given dataset. The model selection process relies on various statistical tests or empirical observations. Once a model is chosen, the parameters of the selected distribution are estimated using parameter estimation methods. The performance of the candidate model on the dataset is then evaluated using one or more fitness-of-fit tests, as described by [60]. This allows for the selection of a fitted distribution that can reasonably serve as a distributional model for the given dataset.

In this study, we apply three probability distributions (Fréchet, Gamma, and Logistic) to the mean indoor temperatures. We employ log-likelihood, Akaike information criterion (AIC), Bayesian information criterion (BIC), and Kolmogorov–Smirnov (K-S) tests to determine the best fit of the probability distribution model(s). The parameters of each model are estimated using the maximum likelihood test. Goodness-of-fit measures are computed to compare the fitted models and identify the best fits. The log-likelihood represents the value of the calculated log-likelihood function based on maximum likelihood parameter estimation. The model with higher log-likelihood values and smaller AIC and BIC values for each selected fitting distribution is considered the best-suited model [61]. Additionally,  $p$ -values are calculated from the K-S statistic for each model to determine if the candidate distribution adequately describes the dataset. A  $p$ -value below 0.05 suggests that the mean indoor data sets are unlikely to be derived from the selected distribution with 95% confidence.

## 3. Results and Discussion

This section highlights the descriptive statistics of the collected data along with data visualization. The outcomes of the correlation analysis and multiple regression models are then presented.

### 3.1. Descriptive Statistics

Table 2 shows the statistical descriptions of PB in cold and hot seasons. In each building, there are five distinct temperatures: the wall, roof, floor, window, and indoor. The mean indoor temperature is 27.1 °C, whereas the other building enclosure temperatures range from 27.8–28.5 °C. The roof demonstrates the highest max temperature of 33.9 °C compared to the rest. In the meantime, during the hot season, the mean indoor temperature is much warmer than the cold season, at 30 °C, which is above the allowable thermal comfort level of 28.6 °C. The same is true for the other building enclosure temperatures, which lie between 30–32 °C. Once more, the roof shows the greatest maximum temperature, which is 38.4 °C, in comparison to the rest. This suggests that among the building enclosure components, the roof may be one of the most important contributors that considerably influence the indoor temperature of PB.

**Table 2.** Descriptive Statistics of PB in Cold Season and Hot Season.

| Temperature (°C)/Building Enclosure | Min.  | Q1    | Median | Mean  | Q3    | Max.  | Variance | Skewness | Kurtosis |
|-------------------------------------|-------|-------|--------|-------|-------|-------|----------|----------|----------|
| Cold Season                         |       |       |        |       |       |       |          |          |          |
| Wall                                | 25.00 | 27.30 | 27.90  | 27.81 | 28.45 | 31.60 | 0.97     | 0.04     | 1.22     |
| Roof                                | 24.70 | 27.50 | 28.30  | 28.46 | 29.30 | 33.90 | 2.34     | 0.76     | 1.29     |
| Floor                               | 23.30 | 27.30 | 28.00  | 27.82 | 28.75 | 30.10 | 1.82     | −1.17    | 1.50     |
| Window                              | 24.80 | 27.60 | 28.50  | 28.49 | 29.40 | 31.10 | 1.67     | −0.40    | −0.10    |
| Indoor                              | 23.40 | 26.60 | 27.30  | 27.1  | 27.90 | 29.50 | 1.11     | −0.53    | 0.20     |
| Hot Season                          |       |       |        |       |       |       |          |          |          |
| Wall                                | 25.80 | 29.32 | 30.80  | 30.48 | 31.90 | 34.50 | 3.62     | −0.29    | −0.53    |
| Roof                                | 24.10 | 30.32 | 32.25  | 32.04 | 34.25 | 38.40 | 9.36     | −0.23    | −0.31    |
| Floor                               | 25.6  | 29.4  | 30.9   | 30.6  | 32.0  | 34.4  | 3.42     | −0.27    | −0.56    |
| Window                              | 26.00 | 30.12 | 32.20  | 31.62 | 33.40 | 37.10 | 6.17     | −0.32    | −0.70    |
| Indoor                              | 24.4  | 28.8  | 30.0   | 30.0  | 31.0  | 33.5  | 3.26     | −0.15    | 0.01     |

Meanwhile, Table 3 provides statistical descriptions of RB during cold and hot seasons. The mean indoor temperature is much higher than that of PB, at 29.7 °C. The other building enclosure's temperatures are similar, hovering about 30 °C. Once more, the roof registers the highest maximum temperature (36.2 °C), but this time, it is closely followed by the window (35.9 °C) and the wall (35.6 °C). During the hot season, the mean indoor temperature is well above 30 °C. The roof reaches 34.1 °C, while the other building enclosure temperatures are all over 31 °C. Additionally, the roof's maximum temperature of 42 °C is exceptionally high, followed by window (39.3 °C) and wall (38.6 °C). This suggests that the most significant factors that significantly affect the indoor temperature of the RB may be the roof, window, and wall.

**Table 3.** Descriptive Statistics of RB in Cold Season and Hot Season.

| Temperature (°C)/Building Enclosure | Min.  | Q1    | Median | Mean  | Q3    | Max.  | Variance | Skewness | Kurtosis |
|-------------------------------------|-------|-------|--------|-------|-------|-------|----------|----------|----------|
| Cold Season                         |       |       |        |       |       |       |          |          |          |
| Wall                                | 24.90 | 28.35 | 30.40  | 30.00 | 31.55 | 35.60 | 5.45     | 0.04     | 1.22     |
| Roof                                | 24.70 | 28.95 | 30.80  | 30.61 | 32.20 | 36.20 | 7.07     | 0.76     | 1.30     |
| Floor                               | 25.00 | 27.80 | 29.20  | 29.12 | 30.40 | 34.20 | 3.46     | −1.17    | 1.50     |
| Window                              | 25.60 | 28.75 | 31.00  | 30.79 | 32.45 | 35.90 | 6.32     | −0.40    | −0.10    |
| Indoor                              | 25.30 | 28.15 | 30.20  | 29.68 | 31.25 | 33.20 | 4.65     | −0.53    | 0.20     |
| Hot Season                          |       |       |        |       |       |       |          |          |          |
| Wall                                | 25.70 | 30.60 | 32.90  | 32.61 | 35.00 | 38.60 | 8.83     | 0.04     | 1.22     |
| Roof                                | 24.0  | 32.2  | 34.5   | 34.1  | 36.6  | 42.0  | 12.90    | 0.76     | 1.30     |
| Floor                               | 26.00 | 30.20 | 31.90  | 31.81 | 33.30 | 36.80 | 4.31     | −1.17    | −0.53    |
| Window                              | 26.10 | 32.30 | 34.30  | 33.76 | 35.80 | 39.30 | 7.21     | −0.40    | −0.10    |
| Indoor                              | 26.0  | 29.2  | 31.9   | 31.6  | 33.9  | 37.3  | 7.79     | −0.53    | 0.20     |

Following that, Figures 2 and 3 provide the boxplots of the PB and RB datasets for cold and hot seasons, respectively. It can be observed that the plots are more spread in RB compared with PB, which indicates a more significant outdoor overheating effect on RB

compared to PB. As presented in our previous study [62], RB's indoor temperature profile frequently mimics that of the outdoor temperature, particularly on sunny-cloudy days, whereas the well-insulated, almost airtight, and optimally shaded PB is always cooler than RB during the daytime. Additionally, outliers that fall outside the whiskers of the boxplot are more visible in the boxplots of PB during the cold and hot seasons and RB during the hot seasons. Outliers can have a significant impact on statistical analyses and can bias the results of statistical models. Due to this, it is necessary to remove these extreme values using Cook's distance approach, which quantifies the impact of individual data points on a regression model and is covered in more detail in the next section.

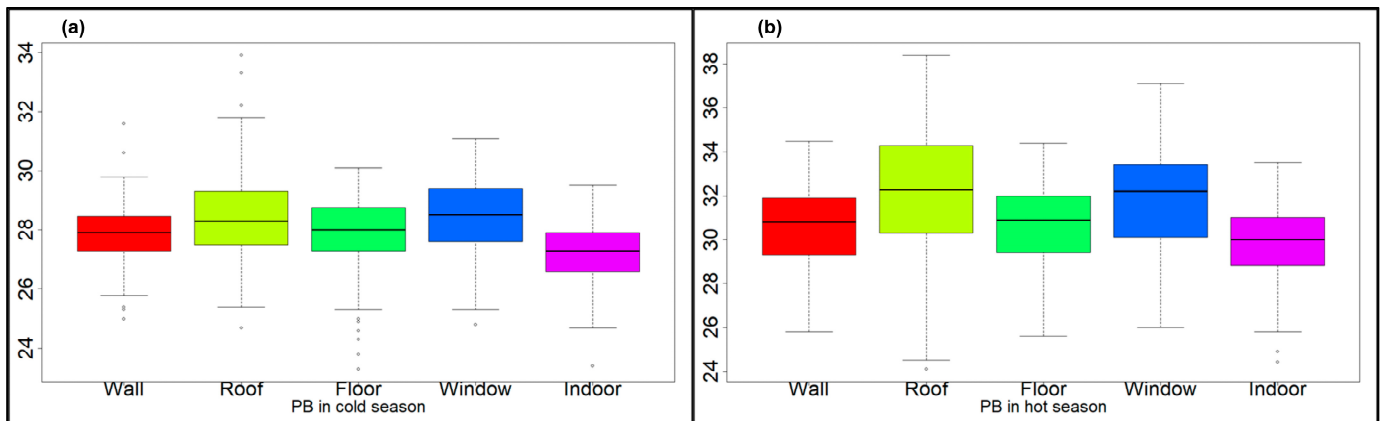


**Figure 2.** Boxplots of the observed PB's temperature distributions during the (a) cold season and (b) hot seasons.

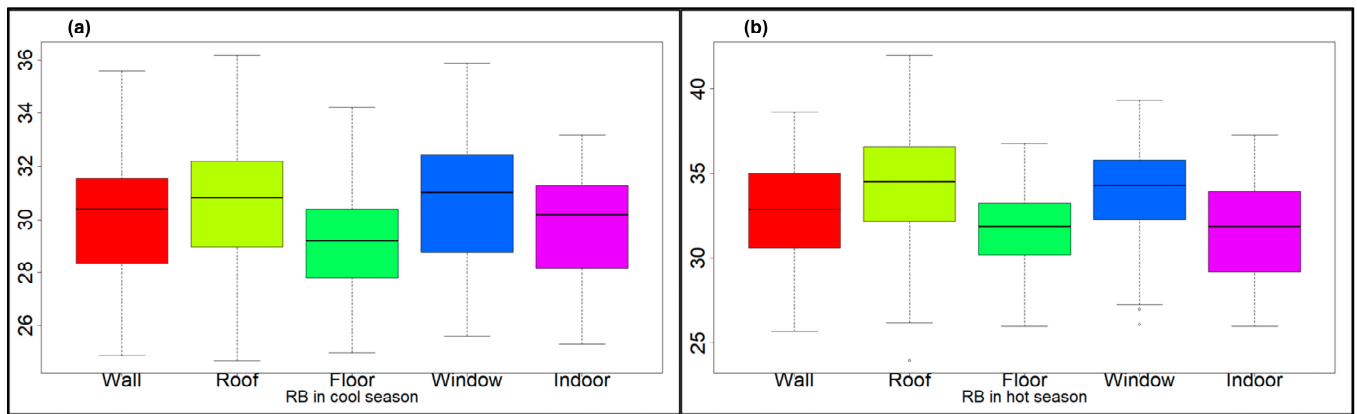


**Figure 3.** Boxplots of the observed RB's temperature distributions during the (a) cold season and (b) hot seasons.

### 3.2. Correlation Analysis of PB and RB Temperature Datasets

Figure 4 shows the results from correlation analysis, which indicated that most of the assessed temperatures were positively correlated with one another at a 1% level of significance. In the cold season, PB's indoor temperature was significantly correlated with window temperature ( $r = 0.76$ ), wall temperature ( $r = 0.75$ ), floor temperature ( $r = 0.64$ ), and roof temperature ( $r = 0.53$ ). The wall temperature shows a strong and positive correlation with window ( $r = 0.72$ ), floor ( $r = 0.69$ ), and roof temperature ( $r = 0.68$ ). The examined roof temperature exhibits a positive correlation with window temperature ( $r = 0.59$ ) and a moderate correlation with floor temperature ( $r = 0.44$ ). Additionally, the analyzed floor temperature indicates a strong and positive correlation with window temperature ( $r = 0.72$ ). These temperature parameters were positively correlated with one another based on a 1% level of significance.

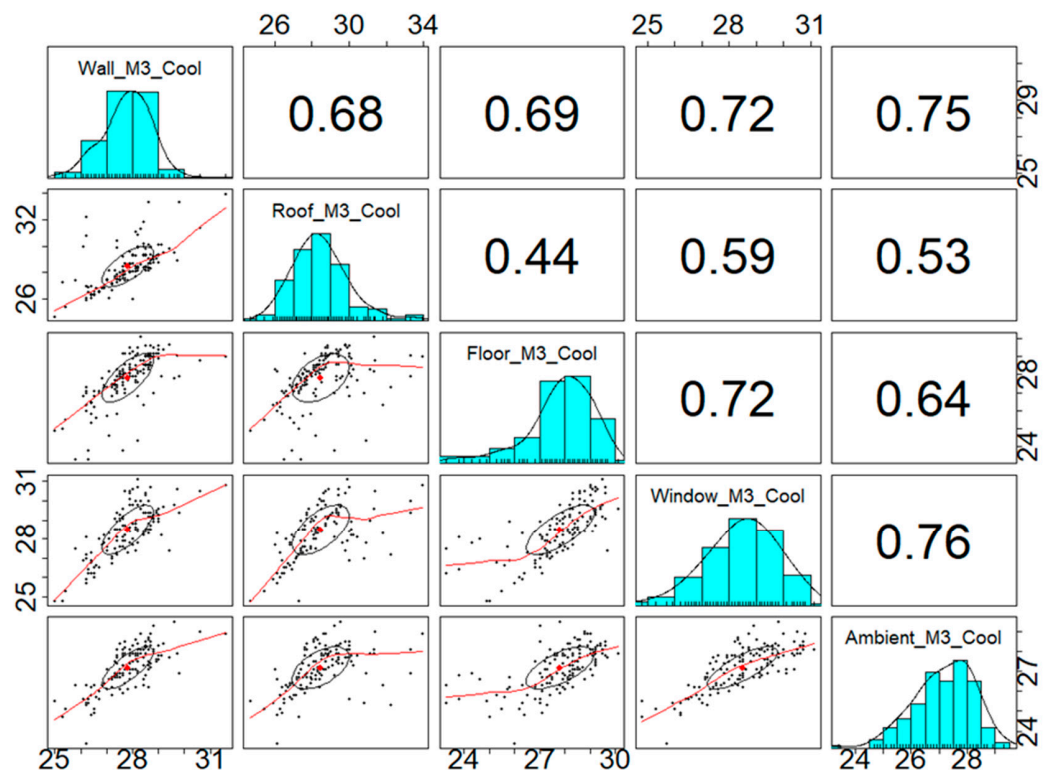


Figure 4. Plots of correlation analysis of PB during the cold season.

Similarly, in the hot season, as shown in Figure 5, the examined indoor temperature was strongly correlated with wall temperature ( $r = 0.80$ ), floor temperature ( $r = 0.76$ ), roof temperature ( $r = 0.72$ ), and window temperature ( $r = 0.70$ ). The wall temperature reveals a significant and strong correlation with floor ( $r = 0.94$ ), window ( $r = 0.88$ ), and roof temperature ( $r = 0.68$ ). The investigated roof temperature exhibits a positive correlation with window temperature ( $r = 0.74$ ) and a strong correlation with floor temperature ( $r = 0.73$ ). Additionally, the assessed floor temperature indicates a significant and positive correlation with window temperature ( $r = 0.91$ ). These temperature parameters were positively correlated with one another based on a 1% level of significance.

In the same vein, Figure 6 shows the results from correlation analysis for RB during the cold season. Figure 6 shows that the indoor temperature was significantly correlated with wall temperature ( $r = 0.82$ ), roof temperature ( $r = 0.80$ ), window temperature ( $r = 0.79$ ), and floor temperature ( $r = 0.67$ ). The wall temperature shows a strong and positive correlation with floor ( $r = 0.76$ ), window ( $r = 0.75$ ), and roof temperature ( $r = 0.75$ ). The investigated roof temperature exhibits a strong and positive correlation with window temperature ( $r = 0.89$ ), and positive correlation with floor temperature ( $r = 0.62$ ). Additionally, the measured floor temperature indicates a positive correlation with window temperature ( $r = 0.59$ ). These temperature parameters were positively correlated with one another based on a 1% level of significance.

Similarly, in the hot season, as shown in Figure 7, the examined indoor temperature was strongly correlated with wall temperature ( $r = 0.84$ ), window temperature ( $r = 0.81$ ), roof temperature ( $r = 0.66$ ), and floor temperature ( $r = 0.65$ ). The wall temperature reveals a significant and strong correlation with window ( $r = 0.87$ ), floor ( $r = 0.82$ ), and roof temperature ( $r = 0.70$ ). The investigated roof temperature exhibits a positive correlation with window temperature ( $r = 0.87$ ) and a strong correlation with floor temperature ( $r = 0.60$ ). Additionally, the assessed floor temperature indicates a positive correlation with window temperature ( $r = 0.72$ ). These temperature parameters were positively correlated with one another based on a 1% level of significance.

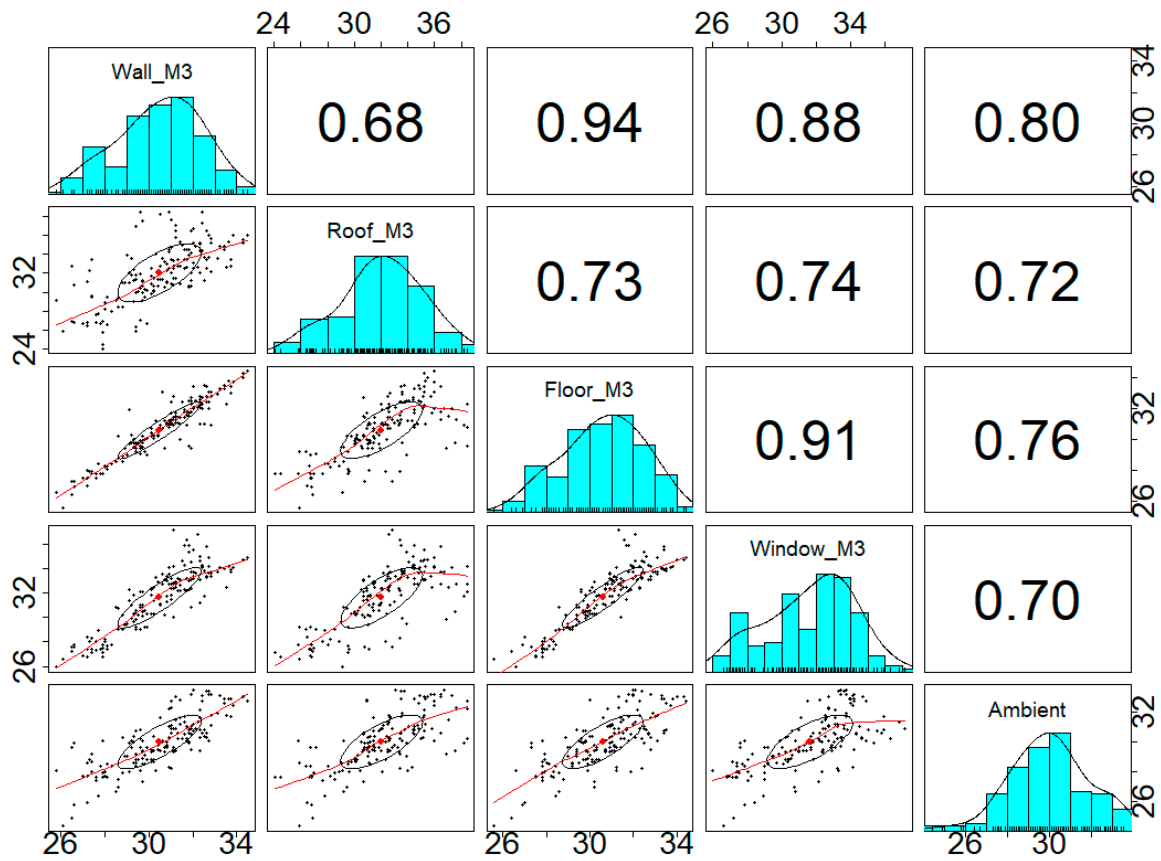


Figure 5. Plots of correlation analysis of PB during the hot season.

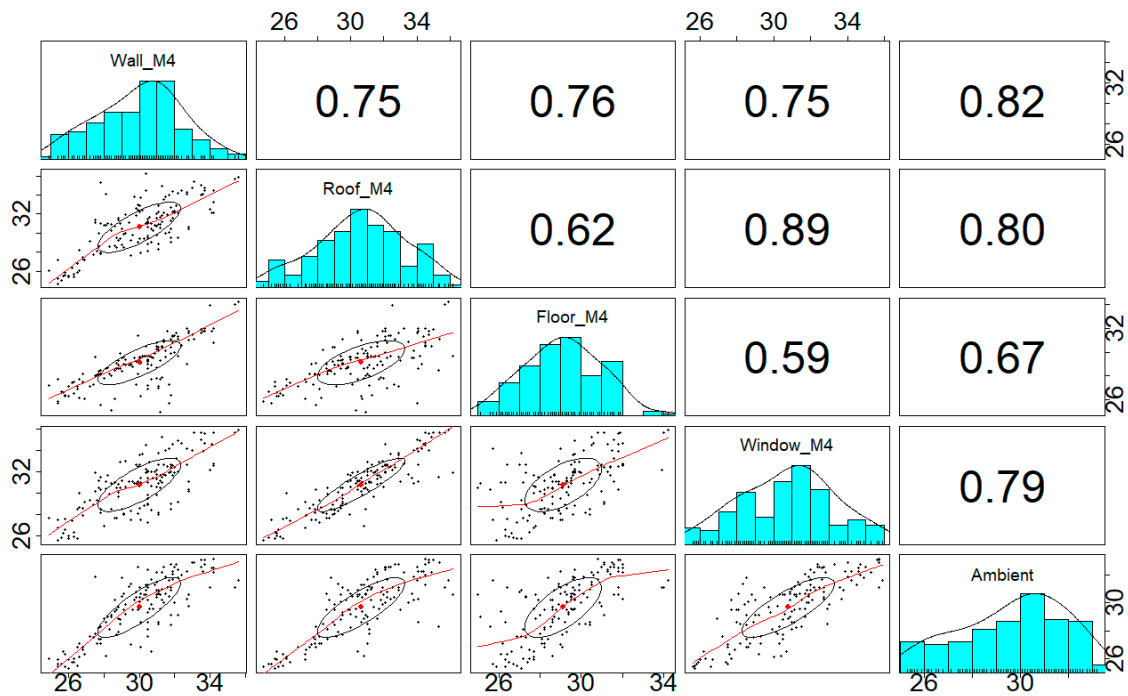


Figure 6. Plots of correlation analysis of RB during the cold season.

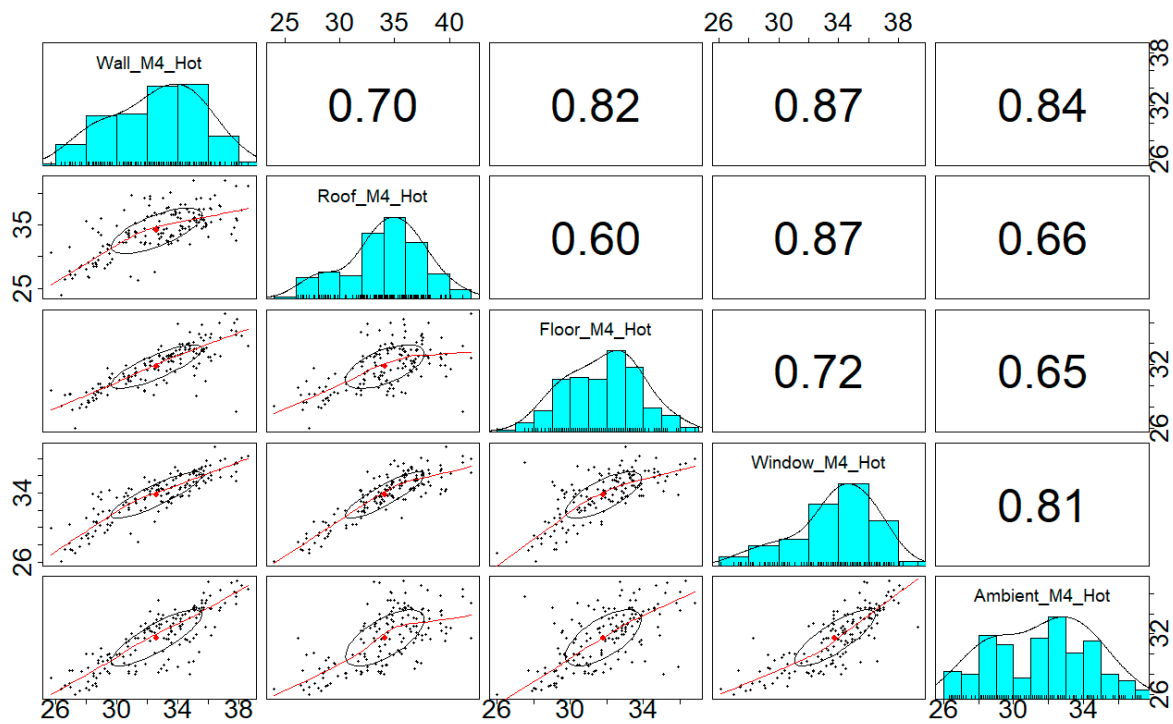


Figure 7. Plots of correlation analysis of RB during the hot season.

### 3.3. Multiple Linear Regression Model

Table 4 provides the results of the multiple regression model for the dataset for PB in the cold season. The  $p$ -value of the overall equation for indoor temperature (Indoor T) is  $2 \times 10^{-16}$ . By referring to the  $\text{Pr}(>|t|)$  values, it is evident that the roof and floor temperatures are not significant since their values are more than 0.05. As a result, we performed additional tests on the training data. The extreme values in the data were removed using Cook’s distance, and we employed a stepwise selection of variables using backward elimination. The variance inflation factor (VIF), which gauges how much a predictor variable’s predicted regression coefficient is inflated by its correlation with other predictor variables in the model, was also used to test for multicollinearity. A common criterion for diagnosing significant collinearity is a VIF score greater than 5. In order to produce a more precise and reliable regression model, strongly correlated variables with  $\text{VIF} \geq 5$  will be eliminated from the final regression model. We will use the same strategy for the other models listed in this section.

$$\text{Indoor } T = \omega_0 + \omega_1 \times \text{Wall} + \omega_2 \times \text{Roof} + \omega_3 \times \text{Floor} + \omega_4 \times \text{Window} \quad (9)$$

Table 4. Results of multiple linear regression model for PB in cold season.

| Parameter | Estimate | Std. Error | t-Statistic | Pr(> t )              |
|-----------|----------|------------|-------------|-----------------------|
| Intercept | 3.65197  | 1.62601    | 2.246       | 0.0267                |
| Wall      | 0.47071  | 0.09073    | 5.188       | $9.79 \times 10^{-7}$ |
| Roof      | -0.05037 | 0.04568    | -1.103      | 0.2726                |
| Floor     | 0.10162  | 0.07029    | 1.446       | 0.1511                |
| Window    | 0.31725  | 0.06920    | 4.584       | $1.21 \times 10^{-5}$ |

R-squared: 0.6727, Adjusted R-squared: 0.6608. F-statistics: 97.873,  $p$ -value:  $2.2 \times 10^{-16} < 1\%$ ,  $p < 0.05$ .

Table 5 shows the fitted regression model for indoor temperature after dropping the roof and floor due to the high  $p$ -value. The F-statistic value increases from 98 to 107, indicating a considerable improvement in the overall fit of the regression model. The root

means squared error (RMSE) for the model on the training and validation sets are 0.8879 and 0.7738, respectively.

$$\text{Indoor } T = \omega_0 + \omega_1 \times \text{Wall} + \omega_4 \times \text{Window} \quad (10)$$

**Table 5.** Results of fitted multiple linear regression model for PB in cold season.

| Parameter | Estimate | Std. Error | t-Statistic | Pr(>  t )             |
|-----------|----------|------------|-------------|-----------------------|
| Intercept | 3.73469  | 1.66021    | 2.249       | 0.0265                |
| Wall      | 0.49196  | 0.07896    | 6.230       | $9.37 \times 10^{-9}$ |
| Window    | 0.34256  | 0.06010    | 5.700       | $1.07 \times 10^{-7}$ |

R-squared: 0.6658, Adjusted R-squared: 0.6596. F-statistics: 106.6, p-value:  $2.2 \times 10^{-16}$ .

Meanwhile, Table 6 depicts the results of the multiple regression model for the dataset for PB in the hot season. For this model, the floor is clearly not significant due to the Pr(> |t|) value more than 0.05. Therefore, it is removed from the final model, along with the window, which is less significant in comparison to the wall and roof, and the results of the newly fitted regression are displayed in Table 7. The model's F-statistic value increases from 89 to 119. The root means squared error (RMSE) for the model on the training and validation sets are 0.8642 and 0.74532, respectively.

$$\text{Indoor } T = \omega_0 + \omega_1 \times \text{Wall} + \omega_2 \times \text{Roof} + \omega_3 \times \text{Floor} + \omega_4 \times \text{Window} \quad (11)$$

**Table 6.** Results of multiple linear regression model for PB in hot season.

| Parameter | Estimate | Std. Error | t-Statistic | Pr(>  t )             |
|-----------|----------|------------|-------------|-----------------------|
| Intercept | 5.92368  | 1.50454    | 3.937       | 0.000136              |
| Wall      | 0.80307  | 0.13789    | 5.824       | $4.56 \times 10^{-8}$ |
| Roof      | 0.27326  | 0.0375     | 6.246       | $6.05 \times 10^{-9}$ |
| Floor     | -0.06152 | 0.15574    | -0.395      | 0.693490              |
| Window    | -0.23035 | 0.08456    | -2.724      | 0.007375              |

R-squared: 0.739, Adjusted R-squared: 0.7307. F-statistics: 88.5, p-value:  $2.2 \times 10^{-16}$ ,  $p < 0.05$ .

**Table 7.** Results of fitted multiple linear regression model for PB in hot season.

| Parameter | Estimate | Std. Error | t-Statistic | Pr(>  t )              |
|-----------|----------|------------|-------------|------------------------|
| Intercept | 5.71005  | 1.39928    | 4.081       | $7.91 \times 10^{-5}$  |
| Wall      | 0.76423  | 0.09636    | 7.931       | $1.01 \times 10^{-12}$ |
| Roof      | 0.26986  | 0.04275    | 6.313       | $4.28 \times 10^{-9}$  |

R-squared: 0.7382, Adjusted R-squared: 0.7325. F-statistics: 118.7, p-value:  $2.2 \times 10^{-16}$ .

Table 7 depicts the fitted regression model for indoor temperature after dropping floor and window due to multicollinearity and  $VIF \geq 5$ . The F-statistic value increases from 88.5 to 118.7, indicating a considerable improvement in the overall fit of the regression model. The RMSE for the model on the training and validation sets are 0.8943 and 0.8271, respectively.

$$\text{Indoor } T = \omega_0 + \omega_1 \times \text{Wall} + \omega_2 \times \text{Roof} \quad (12)$$

Table 8 illustrates the results for RB in the cold season. It is observed that the floor and window temperatures are not significant in this model; hence, it should be dropped from the final model. However, after removing the outliers, the window becomes significant. Table 9 reveals the newly fitted regression model for indoor temperature with wall and

window temperatures with a significantly improved F-statistic value of 228 compared to 85 from the original model. The root means squared error (RMSE) for the model on the training and validation sets are 0.8289 and 0.7078, respectively.

$$\text{Indoor } T = \omega_0 + \omega_1 \times \text{Wall} + \omega_2 \times \text{Roof} + \omega_3 \times \text{Floor} + \omega_4 \times \text{Window} \quad (13)$$

$$\text{Indoor } T = \omega_0 + \omega_1 \times \text{Wall} + \omega_4 \times \text{Window}. \quad (14)$$

**Table 8.** Results of multiple linear regression model for RB in cold season.

| Parameter | Estimate | Std. Error | t-Statistic | Pr(> t )              |
|-----------|----------|------------|-------------|-----------------------|
| Intercept | 4.38802  | 1.59529    | 2.751       | 0.00693               |
| Wall      | 0.37787  | 0.08082    | 4.675       | $8.17 \times 10^{-6}$ |
| Roof      | 0.25043  | 0.08743    | 2.864       | 0.00498               |
| Floor     | 0.07889  | 0.08199    | 0.962       | 0.33801               |
| Window    | 0.12987  | 0.08806    | 1.475       | 0.14303               |

R-squared: 0.7498, Adjusted R-squared: 0.741; F-statistics: 84.67,  $p$ -value:  $2.2 \times 10^{-16} = p < 0.05$ , meaning significant.

**Table 9.** Results of fitted multiple linear regression model for RB in cold season.

| Parameter | Estimate | Std. Error | t-Statistic | Pr(> t )              |
|-----------|----------|------------|-------------|-----------------------|
| Intercept | 3.17044  | 1.25488    | 2.526       | 0.013                 |
| Wall      | 0.54096  | 0.05558    | 9.734       | $2 \times 10^{-16}$   |
| Window    | 0.33546  | 0.05123    | 6.548       | $2.08 \times 10^{-9}$ |

R-squared: 0.8096, Adjusted R-squared: 0.8061. F-statistics: 227.5,  $p$ -value:  $2.2 \times 10^{-16}$ .

Table 10 gives the results for RB in the hot season. The equation of indoor temperature is significant at 1% levels of significance. Again, the F-statistic value for the newly fitted regression model dramatically increases from 89 to 211 after eliminating the roof and floor due to multicollinearity, as shown in Table 11. In both seasons, the final F-statistic values for MLR models estimate the indoor temperature of RB nearly twice those of PB. The root means squared error (RMSE) for the model on the training and validation sets are 0.7998 and 0.6865, respectively.

$$\text{Indoor } T = \omega_0 + \omega_1 \times \text{Wall} + \omega_2 \times \text{Roof} + \omega_3 \times \text{Floor} + \omega_4 \times \text{Window} \quad (15)$$

$$\text{Indoor } T = \omega_0 + \omega_1 \times \text{Wall} + \omega_4 \times \text{Window} \quad (16)$$

**Table 10.** Results of multiple linear regression model for RB in hot season.

| Parameter | Estimate | Std. Error | t-Statistic | Pr(> t )              |
|-----------|----------|------------|-------------|-----------------------|
| Intercept | 5.44434  | 2.39445    | 2.274       | 0.0247                |
| Wall      | 0.65590  | 0.11703    | 5.605       | $1.28 \times 10^{-7}$ |
| Roof      | -0.05332 | 0.07931    | -0.672      | 0.5026                |
| Floor     | -0.19274 | 0.13453    | -1.433      | 0.1545                |
| Window    | 0.37757  | 0.14484    | 2.607       | 0.0103                |

R-squared: 0.7419, Adjusted R-squared: 0.7336. F-statistics: 89.13,  $p$ -value:  $2.2 \times 10^{-16}$ .



**Table 11.** Results of fitted multiple linear regression model for RB in hot season.

| Parameter | Estimate | Std. Error | t-Statistic | Pr(> t )              |
|-----------|----------|------------|-------------|-----------------------|
| Intercept | 1.65056  | 1.56040    | 1.058       | 0.292                 |
| Wall      | 0.51587  | 0.08406    | 6.137       | $1.33 \times 10^{-8}$ |
| Window    | 0.39278  | 0.09571    | 4.104       | $7.79 \times 10^{-5}$ |

R-squared: 0.792, Adjusted R-squared: 0.7882. F-statistics: 211.3,  $p$ -value:  $2.2 \times 10^{-16}$ .

### 3.4. Probability Distributions of Mean Indoor Temperature

One of the key objectives of this study was to examine which probability distribution provides the best fit to the mean indoor temperature of PB and RB during the cold and hot seasons investigated in the warm tropical climate of Malaysia. The probability distributions under consideration include Fréchet, Gamma, and Logistic distributions. The results of fitting three selected distributions (Fréchet, Gamma, and Logistic) to the mean indoor temperature for PB are presented in Table 12. Several statistical measures, including log-likelihood, AIC, BIC, K-S, and  $p$ -values, were used to assess the goodness of fit for each distribution. The fitted Fréchet model exhibits the maximum log-likelihood value among the Gamma and Logistic models for the indoor temperature during the cold season. Conversely, the fitted Logistic model demonstrates the highest log-likelihood value for the indoor temperature during the hot season. Consequently, the Fréchet model is considered the best fit for modeling the indoor temperature in the cold season, while the logistic model is the most suitable for the hot season.

**Table 12.** Estimated parameters, Log-likelihood, AIC, BIC, and K-S for mean indoor temperature for PB in the cold season and hot season, along with competing distributions.

| Distribution        | Fréchet            | Gamma             | Logistic       |
|---------------------|--------------------|-------------------|----------------|
| Cold Season         |                    |                   |                |
| Parameter Estimates | $\alpha = 30.2437$ | $\alpha = 8.9564$ | $\mu = 7.2292$ |
|                     | $\beta = 27.6562$  | $\beta = 3.9574$  | $s = 0.6011$   |
| Log-likelihood      | −217.0127          | −212.9071         | −216.8822      |
| AIC                 | 655.7011           | 663.8857          | 656.5951       |
| BIC                 | 661.8763           | 670.0608          | 662.7703       |
| K-S                 | 0.0465             | 0.0894            | 0.0508         |
| $p$ -value          | 0.8945             | 0.6453            | 0.7856         |
| Hot Season          |                    |                   |                |
| Parameter Estimates | $\alpha = 29.9975$ | $\alpha = 7.4619$ | $\mu = 9.9935$ |
|                     | $\beta = 23.4563$  | $\beta = 3.5462$  | $s = 1.5634$   |
| Log-likelihood      | −326.151           | −325.8505         | −328.2975      |
| AIC                 | 654.3021           | 665.7011          | 646.5951       |
| BIC                 | 660.4773           | 667.8763          | 652.7703       |
| K-S                 | 0.0516             | 0.0665            | 0.0508         |
| $p$ -value          | 0.6585             | 0.5643            | 0.9023         |

To further validate the appropriateness of the fitted distributions, visual inspection using frequency histogram plots was employed. Figure 8 showcases the frequency histogram plots overlaid with the fitted density functions of the Fréchet, Gamma, and Logistic models. The plots clearly indicate that the Fréchet model provides a suitable fit for modeling the indoor temperature during the cold season. Figure 9 shows that the logistic model closely

matches the indoor temperature during the hot season. This visual inspection further supports and confirms the conclusions drawn from the numerical measures.

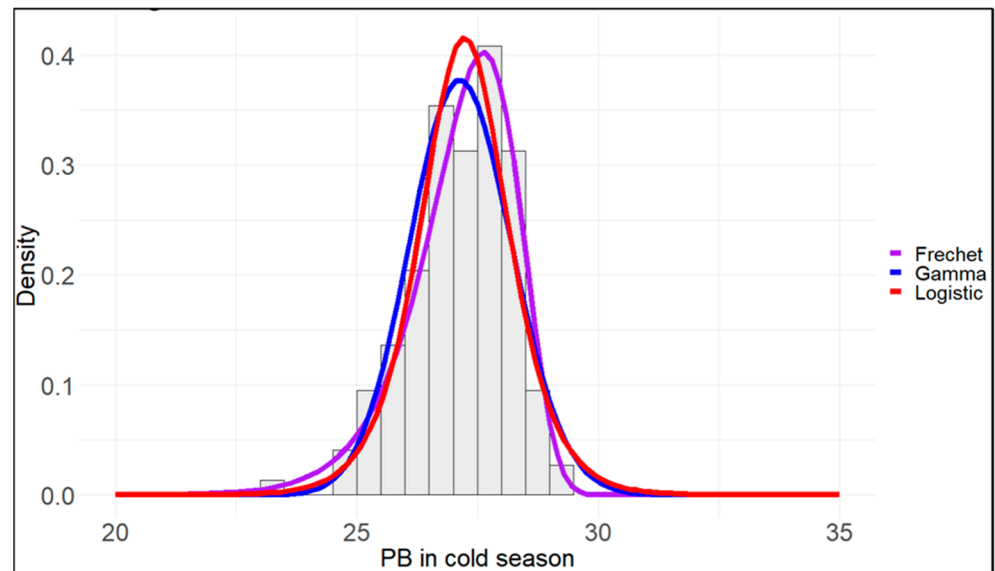


**Figure 8.** Plots of mean indoor temperature for PB in the cold season along with the three fitted Fréchet, Gamma, and Logistic distributions.

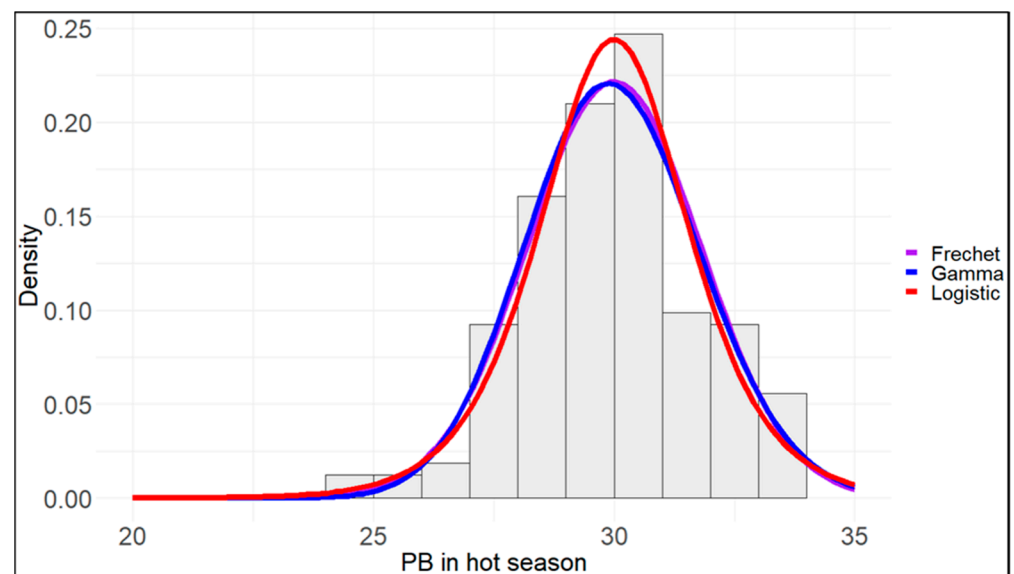


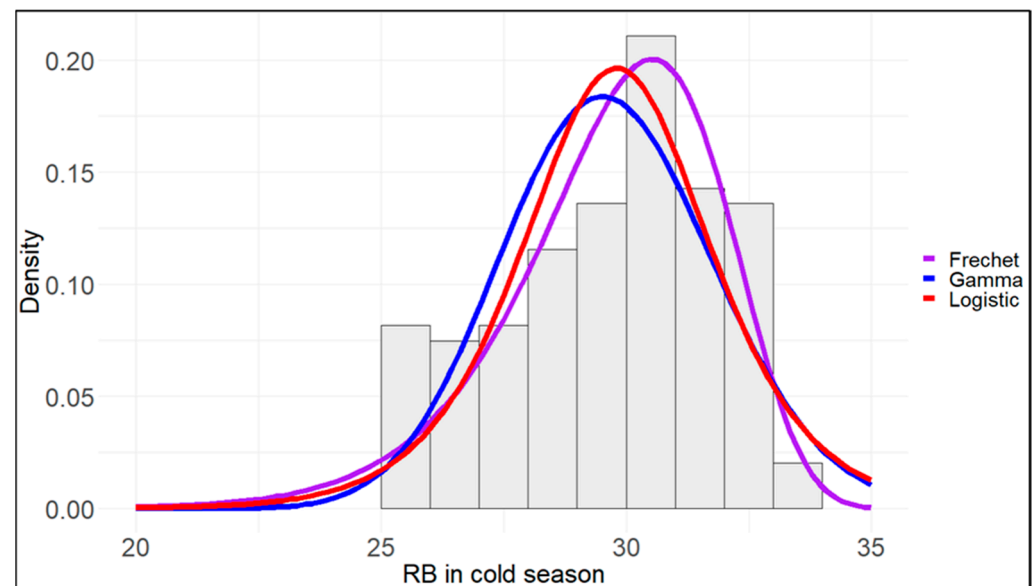
**Figure 9.** Plots of mean indoor temperature for PB in the hot season along with the three fitted Fréchet, Gamma, and Logistic distributions.

Meanwhile, Table 13 displays the outcomes of fitting three chosen continuous distributions (Fréchet, Gamma, and Logistic) to the mean indoor temperature data for RB. Various statistical measures, such as log-likelihood, AIC, BIC, K-S, and  $p$ -values, were employed to evaluate the goodness of fit for each distribution. The Fréchet model demonstrates the highest log-likelihood value among the Gamma and Logistic models for the indoor temperature during the cold season. Conversely, for the hot season, the Logistic model exhibits the highest log-likelihood value. These findings indicate that the Fréchet model is the most appropriate fit for modeling the indoor temperature during the cold season, while the Logistic model is the preferred choice for the hot season.

**Table 13.** Estimated parameters, Log-likelihood, AIC, BIC, and K-S for mean indoor temperature for RB in the cold and hot seasons, along with competing distributions.

| Distribution        | Fréchet            | Gamma             | Logistic       |
|---------------------|--------------------|-------------------|----------------|
| Cold Season         |                    |                   |                |
| Parameter Estimates | $\alpha = 16.6813$ | $\alpha = 6.7654$ | $\mu = 9.8039$ |
|                     | $\beta = 30.6473$  | $\beta = 3.3546$  | $s = 1.2726$   |
| Log-likelihood      | −322.5338          | −316.7914         | −325.7333      |
| AIC                 | 655.7011           | 663.8857          | 656.5951       |
| BIC                 | 661.8763           | 670.0608          | 662.7703       |
| K-S                 | 0.0465             | 0.0893            | 0.0508         |
| <i>p</i> -value     | 0.9045             | 0.6543            | 0.8756         |
| Hot Season          |                    |                   |                |
| Parameter Estimates | $\alpha = 31.6564$ | $\alpha = 8.2930$ | $\mu = 5.6524$ |
|                     | $\beta = 12.6748$  | $\beta = 4.0599$  | $s = 1.6586$   |
| Log-likelihood      | −395.6401          | −395.1029         | −400.9553      |
| AIC                 | 655.7011           | 656.5951          | 654.3021       |
| BIC                 | 661.8763           | 662.7703          | 660.4773       |
| K-S                 | 655.7011           | 656.5951          | 654.3021       |
| <i>p</i> -value     | 0.7564             | 0.6453            | 0.8543         |

To further validate the suitability of the fitted distributions, a visual inspection using frequency histogram plots is conducted. Figure 10 illustrates the frequency histogram plots overlaid with the fitted density functions of the Fréchet, Gamma, and Logistic models. The plots clearly illustrate that the Fréchet model provides a favorable fit for modeling the indoor temperature during the cold season. Figure 11 shows that the logistic model closely aligns with the indoor temperature during the hot season. This visual assessment provides additional support and reinforces the findings obtained from the numerical measures.

**Figure 10.** Plots of mean indoor temperature for RB in the cold season along with the three fitted Fréchet, Gamma, and Logistic distributions.

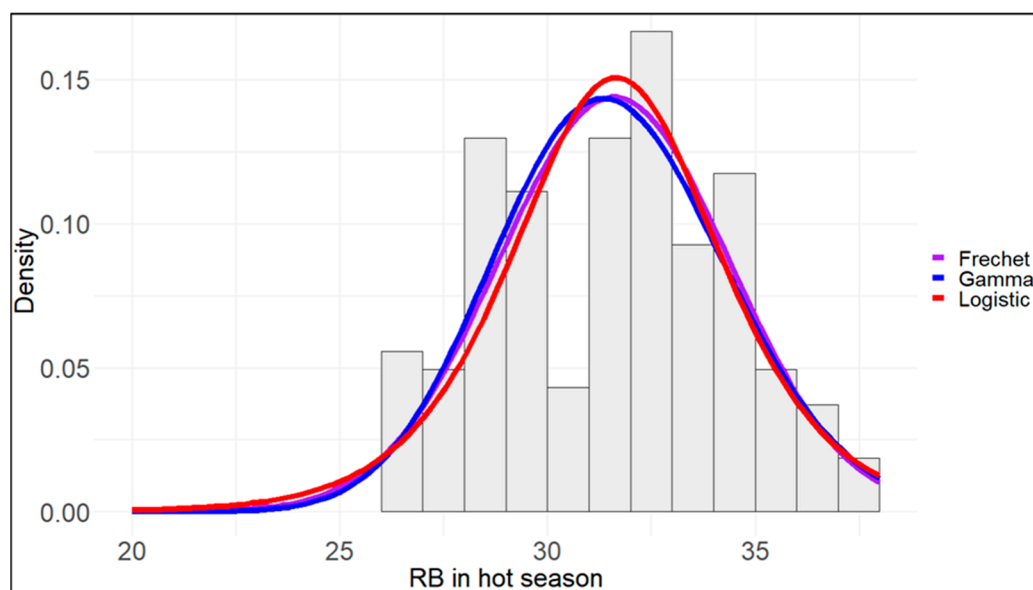


**Figure 11.** Plots of mean indoor temperature for RB in the hot season along with the three fitted Fréchet, Gamma, and Logistic distributions.

### 3.5. Discussion

Overall, it can be deduced from the multiple regression model results that the wall and window majorly influence the indoor temperature of both PB and RB (except for PB in the hot season). The F-statistic values for MLR models to forecast RB indoor temperature are much higher (almost double that of PB) after considering only two factors, wall, and window, and omitting the remaining less significant variables. Windows and walls form the majority of a building's façade; therefore, they play a critical role in maintaining the thermal comfort of a building by preventing the transfer of heat between the interior and exterior environments. Window-to-wall ratio (WWR) is one of the most influencing factors on the energy performance of a building [63]. The study conducted by [64] has established that a WWR of 0.24 is considered ideal to allow optimum indoor daylight and natural ventilation. However, a higher value of WWR could create overheating in the building. Therefore, a careful selection of optimal WWR that balances thermal and visual comfort is critical. Further, the type of material used for the walls, as well as their thickness and insulation, can have a significant impact on the amount of heat that is transferred. For example, materials used in this study with high thermal conductivity, such as sand brick, can allow heat to transfer more easily than materials with lower thermal conductivity, such as clay bricks with double layers. PB has shown a great example of thermal protection against overheating by employing low thermal conductivity materials with a smaller increment of indoor temperature, 10% lower compared to RB during peak days of the hot season.

Windows is another important factor that can affect the indoor temperature of a building. They allow light to enter the building and can provide natural ventilation, but they can also allow heat to enter or escape depending on their orientation, size, and the type of glazing used. For example, windows that face the sun can allow significant transmission of solar radiation, which can significantly inflate building cooling loads compared to those that face away from the sun. Additionally, the type of glazing used can impact the amount of heat transfer. PB is equipped with double glazing with UPVC window frame and external shutters, making it more effective at reducing heat transfer than single glazing with aluminum window frame of RB. The indoor temperature of PB was discovered to be consistently lower than that of RB during the course of the 7-day testing under typical sunny-cloudy weather conditions in our prior study. The double-glazed windows built in PB can withstand the radiation impact of sunshine better than the single-glazed windows installed in RB, resulting in 7% lower window inner surface temperature in PB than in RB. In

addition to double-glazed windows, highly advanced smart windows like electrochromic (EC) windows are gaining popularity and are reported to have significant potential for energy savings and a comfortable environment for people to see outside of a structure [65]. They are made of materials that can be easily switched between a transparent state and a state that is opaque, translucent, and reflective and can be used to regulate the flow of light and radiant heat into or out of a building or other space.

In general, a case-specific analysis based on all the relevant parameters is imperative for the effective implementation of passive energy conservation measures for a given building in a given climate. In warm, humid climates specifically, the reported overall energy savings from incorporating a combination of passive designs range from 10% to 60% [66–68]. Integrating passive building design with a cool roof or green roof can further enhance energy performance. The highest average energy savings reported by cool roofs were 36% in tropical climates [69]. Cool roof, albeit having a higher U-value ( $0.53 \text{ W/m}^2\text{K}$ ) than green roof ( $0.31 \text{ W/m}^2\text{K}$ ), has higher energy performance attributed to the significantly higher solar reflectance. However, from a sustainability or aesthetic perspective, a green roof would be preferable [70].

Recent advancements in technology and materials have made it more accessible and affordable. However, one must ensure that the cost could justify the monetary benefit of energy saving. For example, the insulation gained from the use of insulation plaster such as (ECM 2) and EPS plaster was found to be not economically viable. On the other hand, a steel-reinforced EPS-concrete structure was proposed as a viable, sustainable alternative for conventional pure cement-based structures with an R-value almost eight times higher than that of the normal concrete panel [71]. Extensive studies have proved the promising potential of phase change material (PCM) for energy conservation and thermal management of buildings [72,73]. Aside from the economic factor, one must consider the social, cultural, and environmental implications of contemporary architectural design [74], preferably employing as many locally sourced materials as possible to provide a comprehensive and sustainable approach towards the passive building. Vertical greenery systems or green façades on building envelopes could be considered to provide natural shade, cooling, insulation, and wind barrier benefits [75] in conjunction with a rooftop photovoltaic system to fully utilize the available local renewable energy to increase building energy efficiency [76].

Our results indicated the superiority of Fréchet and Logistic distributions. The Fréchet distribution is found to be the best model for the mean indoor temperature series of PB and RB during the cold season, followed by Logistic and Gamma distributions. On the other hand, our analysis revealed that the logistic distribution provided the best fit for the mean indoor temperature series of PB and RB during the hot season, followed by Fréchet and Gamma distributions. Meanwhile, the Gamma distribution provided the worst fit among all the competing distributions for the mean indoor temperature series of PB and RB during the cold and hot seasons. In another study in Australia, the normal and generalized extreme value distributions provided the best fit to the annual maximum temperature data [16]. Meanwhile, another study in India found that the normal distribution gives the best fit, followed by Log-normal and Gamma distributions to model the annual maximum temperature [24]. In a separate study conducted in Nigeria, it was determined that for modeling the groundwater pollutant concentrations, the odd beta prime Fréchet distribution provided the most accurate fit [77].

#### 4. Conclusions

In this research, we examined the thermal energy performance of a passive building designed for tropical conditions in the warm climate of Malaysia. Throughout various weather conditions, the passive building consistently maintained a lower mean indoor temperature compared to the reference building. The outcomes of the multiple regression analysis demonstrated significant correlations between indoor temperature and wall/window temperatures during colder periods and between indoor temperature and roof/wall/window

temperatures during hotter periods. Notably, clay bricks exhibited superior insulation properties compared to sand bricks, proving especially effective in tropical settings where managing heat and ensuring energy efficiency are paramount. Moreover, their durability and resistance to weathering and moisture make them well-suited for tropical climates, which often experience heavy rainfall and humidity that can impact building materials. However, initial costs may exceed those of sand bricks, and specialized construction expertise is often required for proper installation and support. The same is true for the double-glazed windows used in PB, which have been shown to give far better insulation than single-glazed windows but are relatively more expensive. Thus, a thorough evaluation of the advantages and disadvantages of these materials should inform decision-making. Optimal material choices should consider factors such as regional climate, budgetary constraints, and desired energy efficiency. By incorporating advanced technologies and environmentally conscious practices, creating comfortable living and working environments becomes feasible. Environmentally friendly procedures, comfortable living, and working environments are achievable.

In addition, the findings from the probability distributions exhibited that the Fréchet distribution gave the best fit to the mean indoor temperature series of green and red buildings during the cold season, followed by the Logistic and Gamma distributions. On the other hand, the Logistic distribution provided the best fit for the mean indoor temperature series of green and red buildings during the hot season, followed by the Fréchet and Gamma distributions. It is intended that the findings of this study would guide tropical countries to devise comfortable, cost-effective passive buildings that are green and energy efficient to mitigate global warming. Moving forward, our future studies will employ the r-largest order statistics approach to model the average maximum daily temperatures of passive buildings. This approach is essential for evaluating the potential risks associated with extreme temperatures, and its outcomes will contribute to the development of climate-resilient infrastructure and efficient passive cooling systems.

**Author Contributions:** Conceptualization, S.F.S., A.A.S. and H.D.; Methodology, S.F.S., A.A.S. and H.D.; Software, A.A.S., H.D. and S.F.S.; Validation, A.A.S., M.O., H.D. and R.S.; Supervision, H.D., R.S. and M.O.; Formal analysis, S.F.S., A.A.S., H.D. and K.W.; Writing—original draft, S.F.S. and A.A.S.; Data curation, S.F.S. and K.W.; Writing—review and editing, S.F.S., A.A.S., H.D. and R.S.; Visualization, R.S., K.W., M.O., A.A.S. and H.D. All authors have read and agreed to the published version of the manuscript.

**Funding:** This research received no external funding.

**Institutional Review Board Statement:** Not applicable.

**Informed Consent Statement:** Not applicable.

**Data Availability Statement:** All data that exists in this paper is available from the corresponding author upon request.

**Acknowledgments:** The authors thank PETRONAS Research Sdn. Bhd. for providing the funding to perform the research and publish the findings. Special thanks are due to Universiti Kuala Lumpur (UniKL) for providing the research grant for the construction of the mock-up buildings and collection of experimental data. Further appreciation goes to all 15 sponsors and partners from Malaysia and Singapore who generously provided green building materials or equipment. The second author would also like to thank Universiti Teknologi PETRONAS for sponsoring his PhD studies and offering him a graduate assistant position. Finally, the authors would like to express their gratitude for the referees for their insightful comments.

**Conflicts of Interest:** The authors declare no conflict of interest.

## References

1. O'Brien, T. The IPCC's sixth assessment paper: Hysteria on a global scale. *News Wkly.* **2023**, *3138*, 8.
2. Zakeri, B.; Paulavets, K.; Barreto-Gomez, L.; Echeverri, L.G.; Pachauri, S.; Boza-Kiss, B.; Zimm, C.; Rogelj, J.; Creutzig, F.; Pouya, S.; et al. Pandemic, war, and global energy transitions. *Energies* **2022**, *15*, 6114.

3. IEA. *The Future of Cooling*; IEA: Paris, France, 2018.
4. Kamal, M.A. An overview of passive cooling techniques in buildings: Design concepts and architectural interventions. *Acta Tech. Napoc. Civ. Eng. Archit.* **2012**, *55*, 84–97.
5. Garg, N.K. Passive options for thermal comfort in building envelopes—An assessment. *Sol. Energy* **1991**, *47*, 437–441. [[CrossRef](#)]
6. Mahmud, M.A.; Abir, N.; Ananya, F.R.; Khan, A.N.; Rahman, A.N.M.; Jamine, N. Coir fiber as thermal insulator and its performance as reinforcing material in biocomposite production. *Heliyon* **2023**, *9*, e15597. [[PubMed](#)]
7. Faridul Hasan, K.M.; Hovath, P.G.; Koczan, Z.; Alpar, T. Thermo-mechanical properties of pretreated coir fiber and fibrous chips reinforced multilayered composites. *Nat. Sci. Rep.* **2021**, *11*, 3618.
8. Brose, A.; Jonathan, K.; Leon, G. Coconut Fiber Cement Panels as Wall Insulation and Structural Diaphragm. *Front. Energy Res.* **2019**, *7*, 9.
9. Tuck, N.W.; Zaki, S.A.; Hagishima, A.; Rijal, H.B.; Zakaria, M.A.; Yakub, F. Effectiveness of free running passive cooling strategies for indoor thermal environments: Example from a two-storey corner terrace house in Malaysia. *Build. Environ.* **2019**, *160*, 106214.
10. Zhichao, T.; Zinkai, Z.; Xing, J.; Xin, Z.; Binghui, S.; Xing, S. Towards adoption of building energy simulation and optimization for passive building design: A survey and a review. *Energy Build.* **2018**, *158*, 1306–1316.
11. Kang, J.E.; Ahn, K.U.; Park, C.S.; Shuetze, T. Assessment of Passive vs. Active Strategies for a School Building Design. *Sustainability* **2015**, *7*, 15136–15151.
12. Lee, K.S.; Oberdick, W.A. Development of a passive solar simulation technique using small scale models. *Sol. World Forum* **1981**, *3*, 1803–1810.
13. Grimmer, D.P.; McFarland, R.D.; Balcomb, J.D. Initial experimental tests on the use of small passive solar boxes to model the thermal performance of passively solar-heated building designs. *Sol. Energy* **1979**, *22*, 351–354. [[CrossRef](#)]
14. Athienitis, A.K.; Ramadan, H. Numerical model of a building with transparent insulation. *Sol. Energy* **2000**, *67*, 101–109. [[CrossRef](#)]
15. Suleiman, A.A.; Daud, H.; Othman, M.; Ishaq, A.I.; Indawati, R.; Abdullah, M.L.; Hussin, A. The Odd Beta Prime-G Family of Probability Distributions: Properties and Applications to Engineering and Environmental Data. *Comput. Sci. Math. Forum* **2023**, *7*, 20.
16. Haddad, K. Selection of the best fit probability distributions for temperature data and the use of L-moment ratio diagram method: A case study for NSW in Australia. *Theor. Appl. Climatol.* **2021**, *143*, 1261–1284. [[CrossRef](#)]
17. Hossain, M. Fitting the probability distribution of monthly maximum temperature of some selected stations from the northern part of Bangladesh. *Int. J. Ecol. Econ. Stat.* **2018**, *39*, 80–91.
18. Hossian, M.M.; Abdulla, F.; Rahman, M.H. Selecting the probability distribution of monthly maximum temperature of Dhaka (capital city) in Bangladesh. *Jahangirnagar Univ. J. Stat. Stud.* **2016**, *33*, 33–45.
19. Nemukula, M.M.; Sigauke, C. Modelling average maximum daily temperature using r largest order statistics: An application to South African data. *Jambá J. Disaster Risk Stud.* **2018**, *10*, 1–11. [[CrossRef](#)]
20. Guayjaremanishk, P.; Busababodhin, P.; Chiangpradit, M.; Papukdee, N.; Ruechairam, J.; Ruanthaisong, K. Extreme Value Modeling of Daily Maximum Temperature with the r-Largest Order Statistics. *J. Appl. Sci. Emerg. Technol.* **2021**, *20*, 28–38.
21. Shakil, M.; Sirajo, M.; Khadim, A.; Aliyu, M.A.; Singh, J.; Kibria, B. Probability Modeling of Lifetime and Temperature Data of the Black Holes existing in X-Ray Binaries. *World Sci. News* **2022**, *173*, 78–93.
22. Al-Hemyari, Z.A.; Abbasi, J.N.A. Modelling and analysing the daily temperature of several cities using mixture Gaussian distributions. *Int. J. Comput. Sci. Math.* **2023**, *17*, 320–341. [[CrossRef](#)]
23. Chen, D.; Chen, X.; Wang, J.; Zhang, Z.; Wang, Y.; Jia, C.; Hu, X. Estimation of thermal time model parameters for seed germination in 15 species: The importance of distribution function. *Seed Sci. Res.* **2021**, *31*, 83–90. [[CrossRef](#)]
24. Poonia, N.; Azad, S. Projection of annual maximum temperature over Northwest Himalayas using probability distribution models. *Theor. Appl. Climatol.* **2022**, *149*, 1599–1627. [[CrossRef](#)]
25. Moccia, B.; Mineo, C.; Ridolfi, E.; Russo, F.; Napolitano, F. Probability distributions of daily rainfall extremes in Lazio and Sicily, Italy, and design rainfall inferences. *J. Hydrol. Reg. Stud.* **2021**, *33*, 100771. [[CrossRef](#)]
26. Pawar, U.V.; Hire, P.S.; Gunjal, R.P.; Patil, A.D. Modeling of magnitude and frequency of floods on the Narmada River: India. *Model. Earth Syst. Environ.* **2020**, *6*, 2505–2516. [[CrossRef](#)]
27. Umar, S.; Lone, M.A.; Goel, N.K. Modeling of peak discharges and frequency analysis of floods on the Jhelum river, North Western Himalayas. *Model. Earth Syst. Environ.* **2021**, *7*, 1991–2003. [[CrossRef](#)]
28. Ozonur, D.; Pobocikova, I.; de Souza, A. Statistical analysis of monthly rainfall in Central West Brazil using probability distributions. *Model. Earth Syst. Environ.* **2021**, *7*, 1979–1989. [[CrossRef](#)]
29. Kousar, S.; Khan, A.R.; Hassan, M.U.; Noreen, Z.; Bhatti, S.H. Some best-fit probability distributions for at-site flood frequency analysis of the Ume River. *J. Flood Risk Manag.* **2020**, *13*, e12640. [[CrossRef](#)]
30. Haq, M.A.U.; Chand, S.; Sajjad, M.Z.; Usman, R.M. Evaluating the suitability of two parametric wind speed distributions: A case study from Pakistan. *Model. Earth Syst. Environ.* **2021**, *7*, 1683–1691. [[CrossRef](#)]
31. Pobočková, I.; Sedláčková, Z.; Michalková, M. Application of Four Probability Distributions for Wind Speed Modeling. *Procedia Eng.* **2017**, *192*, 713–718. [[CrossRef](#)]
32. Singh, V.V.; Suleman, A.A.; Ibrahim, A.; Abdullahi, U.A.; Suleiman, S.A. Assessment of probability distributions of groundwater quality data in Gwale area, north-western Nigeria. *Ann. Optim. Theory Pract.* **2020**, *3*, 37–46.

33. Auwalu, I.; Abubakar, S.A.; Aliyu, A.U.; Abubakar, S.S. Monitoring Groundwater Quality using Probability Distribution in Gwale, Kano state, Nigeria. *J. Stat. Model. Anal.* **2021**, *3*, 2. Available online: <http://jummec.um.edu.my/index.php/JOSMA/article/view/32362> (accessed on 26 June 2023).
34. Ogarekpe, N.M.; Tenebe, I.T.; Emenike, P.C.; Udodi, O.A.; Antigha, R.E. Assessment of regional best-fit probability density function of annual maximum rainfall using CFSR precipitation data. *J. Earth Syst. Sci.* **2020**, *129*, 176. [[CrossRef](#)]
35. Poonia, N.; Azad, S. A New Exponentiated Generalized Linear Exponential Distribution: Properties and Application. *RMS Res. Math. Stat.* **2021**, *8*, 1953233. [[CrossRef](#)]
36. Amin, M.T.; Rizwan, M.; Alazba, A.A. A best-fit probability distribution for the estimation of rainfall in northern regions of Pakistan. *Open Life Sci.* **2016**, *11*, 432–440. [[CrossRef](#)]
37. Gado, T.A.; Salama, A.M.; Zeidan, B.A. Selection of the best probability models for daily annual maximum rainfalls in Egypt. *Theor. Appl. Climatol.* **2021**, *144*, 1267–1284. [[CrossRef](#)]
38. Mamoon, A.A.; Rahman, A. Selection of the best fit probability distribution in rainfall frequency analysis for Qatar. *Nat. Hazards* **2017**, *86*, 281–296. [[CrossRef](#)]
39. Morgan, E.C.; Lackner, M.; Vogel, R.M.; Baise, L.G. Probability distributions for offshore wind speeds. *Energy Convers. Manag.* **2011**, *52*, 15–26. [[CrossRef](#)]
40. Dookie, I.; Roche, S.; Singh, A.; Ramlal, C.J. Evaluating wind speed probability distribution models with a novel goodness of fit metric: A Trinidad and Tobago case study. *Int. J. Energy Environ. Eng.* **2018**, *9*, 323–339. [[CrossRef](#)]
41. Gocic, M.; Velimirovic, L.; Stankovic, M.; Trajkovic, S. Determining the best fitting distribution of annual precipitation data in Serbia using L-moments method. *Earth Sci. Inform.* **2021**, *14*, 633–644. [[CrossRef](#)]
42. Alam, M.A.; Emura, K.; Farnham, C.; Yuan, J. Best-Fit Probability Distributions and Return Periods for Maximum Monthly Rainfall in Bangladesh. *Climate* **2018**, *6*, 9. [[CrossRef](#)]
43. Wang, Y.; Wang, Z.; Zhang, Z.; Shen, D.; Zhang, L. The best-fitting distribution of water balance and the spatiotemporal characteristics of drought in Guizhou Province, China. *Theor. Appl. Climatol.* **2021**, *143*, 1097–1112. [[CrossRef](#)]
44. De Michele, C.; Avanzi, F. Superstatistical distribution of daily precipitation extremes: A worldwide assessment. *Sci. Rep.* **2018**, *8*, 14204. [[CrossRef](#)] [[PubMed](#)]
45. Młyński, D.; Wałęga, A.; Petroselli, A.; Tauro, F.; Cebulska, M. Estimating Maximum Daily Precipitation in the Upper Vistula Basin, Poland. *Atmosphere* **2019**, *10*, 43. [[CrossRef](#)]
46. Mamoon, A.A.; Joergensen, N.E.; Rahman, A.; Qasem, H. Derivation of new design rainfall in Qatar using L-moment based index frequency approach. *Int. J. Sustain. Built Environ.* **2014**, *3*, 111–118. [[CrossRef](#)]
47. Sharma, M.A.; Singh, J.B. Use of probability distribution in rainfall analysis. *N. Y. Sci. J.* **2010**, *3*, 40–49.
48. Kwaku, X.S.; Duke, O. Characterization and frequency analysis of one day annual maximum and two to five consecutive days maximum rainfall of Accra, Ghana. *ARN J. Eng. Appl. Sci.* **2007**, *2*, 27–31.
49. Lazoglou, G.; Anagnostopoulou, C.; Tolika, K.; Kolyva-Machera, F. A review of statistical methods to analyze extreme precipitation and temperature events in the Mediterranean region. *Theor. Appl. Climatol.* **2019**, *136*, 99–117. [[CrossRef](#)]
50. Suleiman, A.A.; Daud, H.; Singh, N.S.S.; Othman, M.; Ishaq, A.I.; Sökkalingam, R. A Novel Odd Beta Prime-Logistic Distribution: Desirable Mathematical Properties and Applications to Engineering and Environmental Data. *Sustainability* **2023**, *15*, 10239. [[CrossRef](#)]
51. Ishaq, A.I.; Abiodun, A.A. The Maxwell–Weibull Distribution in Modeling Lifetime Datasets. *Ann. Data Sci.* **2020**, *7*, 639–662. [[CrossRef](#)]
52. Ishaq, A.; Usman, A.; Tasi’u, M.; Suleiman, A.; Ahmad, A. A New Odd F-Weibull Distribution: Properties and Application of the Monthly Nigerian Naira to British Pound Exchange Rate Data. In Proceedings of the 2022 International Conference on Data Analytics for Business and Industry (ICDABI), Virtual, 25–26 October 2022; pp. 326–332.
53. Suleiman, A.A.; Ibrahim, A.; Abdullahi, U.A. Statistical explanatory assessment of groundwater quality in Gwale LGA, Kano state, northwest Nigeria. *Hydrospatial Anal.* **2020**, *4*, 1–13. [[CrossRef](#)]
54. Malakootian, M.; Ahmadian, M. Ciprofloxacin removal by electro-activated persulfate in aqueous solution using iron electrodes. *Appl. Water Sci.* **2019**, *9*, 140. [[CrossRef](#)]
55. Saleem, A.; Dandigi, M.N.; Kumar, K.V. Correlation-regression model for physico-chemical quality of groundwater in the South Indian city of Gulbarga. *Afr. J. Environ. Sci. Technol.* **2012**, *6*, 353–364. [[CrossRef](#)]
56. El-Mejri, H.; Moussa, A.B.; Salem, S.H.; Zouari, K. *Hydrochemical Investigation and Quality Assessment of Groundwater in the BouHafna-Haffouz Unconfined Aquifers, Central Tunisia. Aquifers-Matrix and Fluids: Tunisia*; IntechOpen: London, UK, 2018.
57. Suleiman, A.A. Analysis of multicollinearity in multiple regressions. *Int. J. Adv. Technol. Eng. Sci.* **2015**, *3*, 571–578.
58. Galwey, N.W. *Introduction to Mixed Modelling: Beyond Regression and Analysis of Variance*; John Wiley & Sons: Hoboken, NJ, USA, 2014.
59. Galecki, A.; Burzykowski, T. *Linear Mixed-Effects Mode, in Linear Mixed-Effects Models Using R*; Springer: Berlin/Heidelberg, Germany, 2013; pp. 245–273.
60. Maryam, G.; Kaveh, O.; Saed, E.; Vijay, P.S. Analyzing the groundwater quality parameters using frequency analysis. *Am. J. Eng. Appl. Sci.* **2018**, *11*, 482–490.
61. Abdullahi, U.A.; Suleiman, A.A.; Ishaq, A.I.; Suleiman, A. The Maxwell–Exponential Distribution: Theory and Application to Lifetime Data. *J. Stat. Model. Anal.* **2021**, *3*, 2. [[CrossRef](#)]



62. Wagner, K.; Salleh, S.F.; Ayodele, B.V. Tropically Adapted Passive Building: The Impact of Building Design and Double Glazing on Ambient Temperature and Windows' Inner Surface Temperature. In Proceedings of the International Conference on Industrial Engineering and Operations Management, Dubai, United Arab Emirates, 10–12 March 2020.
63. Sayadi, S.; Hayati, A.; Salmanzadeh, M. Optimization of Window-to-Wall Ratio for Buildings Located in Different Climates: An IDA-Indoor Climate and Energy Simulation Study. *Energies* **2021**, *7*, 1974. [[CrossRef](#)]
64. Melo, A.P.; Sorgato, M.J.; Lamberts, R. Building Energy Performance Assessment: Comparison between ASHRAE Standard 90.1 and Brazilian Regulation. *Energy Build.* **2014**, *70*, 372–383. [[CrossRef](#)]
65. Budaiwi, I.M.; Fasi, M.A. Assessing the Energy-Saving Potential and Visual Comfort of Electrochromic Smart Windows in Office Buildings: A Case Study in Dhahran, Saudi Arabia. *Sustainability* **2023**, *15*, 9632. [[CrossRef](#)]
66. Ahsan, T. Passive Design Features for Energy-Efficient Residential Buildings in Tropical Climates: The Context of Dhaka, Bangladesh. Master's Thesis, KTH Architecture and the Built Environment, Stockholm, Sweden, 2009.
67. Nematchoua, M.K.; Vanona, J.C.; Orosa, J.A. Energy efficiency and thermal performance of office buildings integrated with passive strategies in coastal regions of humid and hot tropical climates in Madagascar. *Appl. Sci.* **2020**, *10*, 7. [[CrossRef](#)]
68. Sharma, L.; Lal, K.K.; Rakshit, D. Evaluation of impact of passive design measures with energy saving potential through estimation of shading control for visual comfort. *J. Build Phys.* **2018**, *42*, 220–238. [[CrossRef](#)]
69. Rawat, M.; Singh, R.N. A study on the comparative review of cool roof thermal performance in various regions. *Energy Built Environ.* **2022**, *3*, 327–347. [[CrossRef](#)]
70. Mujeebo, M.A.; Bano, F. Integration of passive energy conservation measures in a detached residential building design in warm humid climate. *Energy* **2022**, *255*, 124587. [[CrossRef](#)]
71. Raj, R.; Nayak, K.; Akbari, A.; Saha, P. Prospects of expanded polystyrene sheet as green building material. *Int. J. Civ. Eng. Res.* **2014**, *5*, 145–150.
72. Al-Yasiri, Q.; Szabo, M. Experimental evaluation of the optimal position of a macroencapsulated phase change material incorporated composite roof under hot climate conditions. *Sustain. Energy Technol. Assess.* **2021**, *45*, 101121. [[CrossRef](#)]
73. Beemkumar, N.; Yuvarajan, D.; Arulprakasajothi, M.; Ganesan, S.; Elangovan, K.; Senthilkumar, G. Experimental investigation and numerical modeling of room temperature control in buildings by the implementation of phase change material in the roof. *J. Sol. Energy Eng. Trans. E* **2020**, *142*, 011011. [[CrossRef](#)]
74. Beyaz, C.; Ercin, C. Evaluation of Modern Architecture Criteria in the Context of Sustainability and Architectural Approach; Modern Period in North Nicosia. *Sustainability* **2023**, *15*, 10005. [[CrossRef](#)]
75. Blanco, I.; Convertino, F. Thermal Performance of Green Façades: Research Trends Analysis Using a Science Mapping Approach. *Sustainability* **2023**, *15*, 9981. [[CrossRef](#)]
76. Liao, X.; Wang, W.; Zhou, Y. Investigating the Energy-Saving Effectiveness of Envelope Retrofits and Photovoltaic Systems: A Case Study of a Hotel in Urumqi. *Sustainability* **2023**, *15*, 9926. [[CrossRef](#)]
77. Suleiman, A.A.; Daud, H.; Othman, O.; Singh, N.S.S.; Ishaq, A.I.; Sockalingam, R.; Husin, A. A Novel Extension of the Fréchet Distribution: Statistical Properties and Application to Groundwater Pollutant Concentrations. *J. Data Sci. Insights* **2023**, *1*, 8–24.

**Disclaimer/Publisher's Note:** The statements, opinions and data contained in all publications are solely those of the individual author(s) and contributor(s) and not of MDPI and/or the editor(s). MDPI and/or the editor(s) disclaim responsibility for any injury to people or property resulting from any ideas, methods, instructions or products referred to in the content.